Geophys. J. Int. (2009) doi: 10.1111/j.1365-246X.2009.04342.x

Three-dimensional *P*-wave velocity structure on the shallow part of the Central Costa Rican Pacific margin from local earthquake tomography using off- and onshore networks

I. G. Arroyo,[1] S. Husen,[2] E. R. Flueh,[1] J. Gossler,[1] E. Kissling[2] and G. E. Alvarado[3]

[1]*Leibniz Institute for Marine Science (IfM-Geomar) and* SFB574*, Kiel, Germany. E-mail: iarroyo@ifm-geomar.de*
[2]*Swiss Federal Institute of Technology Zurich, ETH Hoenggerberg, Zurich, Switzerland*
[3]*Instituto Costarricense de Electricidad (ICE) and Universidad de Costa Rica, San José, Costa Rica (Red Sismológica Nacional-RSN)*

Accepted 2009 July 21. Received 2009 June 21; in original form 2008 April 25

SUMMARY

The Central Costa Rican Pacific margin is characterized by a high-seismicity rate, coincident with the subduction of rough-relief ocean floor and has generated earthquakes with magnitude up to seven in the past. We inverted selected *P*-wave traveltimes from earthquakes recorded by a combined on- and offshore seismological array deployed during 6 months in the area, simultaneously determining hypocentres and the 3-D tomographic velocity structure on the shallow part of the subduction zone (<70 km). The results reflect the complexity associated to subduction of ocean-floor morphology and the transition from normal to thickened subducting oceanic crust. The subducting slab is imaged as a high-velocity perturbation with a band of low velocities (LVB) on top encompassing the intraslab seismicity deeper than ∼30 km. The LVB is locally thickened by the presence of at least two subducted seamounts beneath the margin wedge. There is a general eastward widening of the LVB over a relatively short distance, closely coinciding with the onset of an inverted forearc basin onshore and the appearance of an aseismic low-velocity anomaly beneath the inner forearc. The latter coincides spatially with an area of the subaerial forearc where differential uplift of blocks has been described, suggesting tectonic underplating of eroded material against the base of the upper plate crust. Alternatively, the low velocities could be induced by an accumulation of upward migrating fluids. Other observed velocity perturbations are attributed to several processes taking place at different depths, such as slab hydration through outer rise faulting, tectonic erosion and slab dehydration.

Key words: Seismic tomography; Subduction zone processes; Continental margins: convergent; Crustal structure.

1 INTRODUCTION

The convergent margin along the Middle America Trench (MAT) off Costa Rica and Nicaragua has been the focus during the first stage of the project SFB574 'Volatiles and Fluids in Subduction Zones', which aims to better understand the processes involved in the exchange of fluids in erosional convergent margins. The diversity in structure and morphology of the incoming Cocos Plate and its associated effects on the structure of the margin, such as variations in the subduction angle, depth of the Wadati-Benioff seismicity, deformation style, plate coupling and magmatic composition along the volcanic front, confer special interest to the area.

Being a direct response to the dynamics and structure of subduction zones, their seismicity and velocity structure provide valuable insights into the processes taking place in these regions, where more than 80 per cent of the seismic energy of the Earth is released. Local earthquake tomography (LET) is one of the most powerful methods to obtain precise local earthquake locations and detailed knowledge of the 3-D velocity field, as proved in this (Protti *et al.* 1996; Husen *et al.* 2003a; DeShon *et al.* 2006) and other subduction zones.

The Central Pacific region of Costa Rica displays a very high-seismicity rate, coinciding with the subduction of rough-relief ocean floor, which includes seamounts and plateaus (Fig. 1). The area has generated earthquakes with magnitude up to seven in the past, most recently a M_w 6.9 event in 1999 and a M_w 6.4 in 2002. As part of the SFB574, an 'amphibious' network, consisting of land and ocean-bottom stations, was installed in the area for a period of 6 months. Since commonly the trench and forearc regions of subduction zones are located offshore, the availability of ocean-bottom hydrophones offers an excellent opportunity to study the shallower part of the margin. This makes the determination of high-quality hypocentre locations possible for the first time in this area, where the quality and completeness of the seismic catalogues from the two permanent countrywide networks is impaired by the lack of coverage offshore.

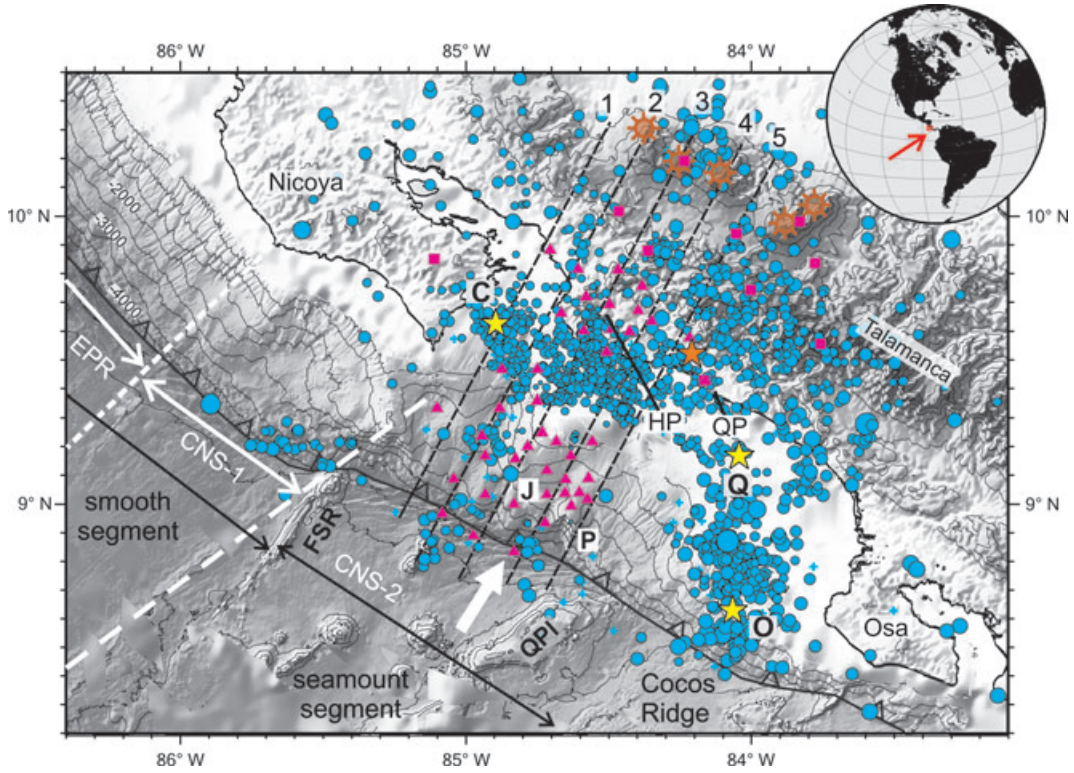

Figure 1. Setting of the Jacó seismological experiment in the Central Pacific margin of Costa Rica. The network (triangles) consisted of land and ocean-bottom stations that operated from 2002 April to October; additional readings from land stations of the permanent network RSN (red squares) improved the coverage. Total recorded seismicity during the experiment is shown (blue circles). Dashed lines denote the location of vertical cross-sections shown in Fig. 14. Bathymetry (exaggerated), including contours every 500 m, and main tectonic segments after von Huene *et al*. (2000) and Barckhausen *et al*. (2001), respectively. Cocos Plate oceanic crust was formed at the East Pacific Rise (EPR) and at the Cocos-Nazca Spreading Center (CNS). Cocos Plate motion azimuth (thick white arrow) from DeMets *et al*. (1994). Radiating circles denote Holocene volcanoes in central Costa Rica. Yellow stars represent the epicentres of recent large earthquakes associated to subduction of bathymetric highs: C: 1990 M_w 7.0 Cóbano (Husen *et al*. 2002), Q: 1999 M_w 6.9 Quepos (location from Universidad Nacional de Costa Rica) and O: 2002 M_w 6.4 Osa (preliminary location from Jacó and RSN networks combined). Orange star: upper-plate, 2004 M_w 6.4 Damas earthquake (Pacheco *et al*. 2006). HP: Herradura Promontory, QP: Quepos Promontory, FSR: Fisher Seamount and Ridge, QPl: Quepos Plateau, J: Jacó Scar and P: Parrita Scar.

The main goals of the experiment include the characterization of the seismicity in this portion of the margin and its correlation with the tectonic and velocity structure, with emphasis on the seismogenic zone, that is, the zone were the overriding and subducting plates are coupled. Foregoing studies lacked the coverage necessary to define the limits of the interplate seismicity, which are essential for the definition of the seismogenic zone and the process controlling its extent. The Costa Rican Central Pacific margin provides also the possibility of studying the effects of seamounts at different stages of subduction on seismicity, velocity structure and the seismogenic zone. Moreover, with most of the seismogenic zone research carried out to date in accretionary margins, the results of this and similar experiments in the area could augment our understanding of the processes taking place in tectonically erosive margins, as well as the characteristics common to both margin types.

Furthermore, the Costa Rican margin has been the target of several controlled-source seismology (CSS) campaigns for more than 30 yr. In addition to swath bathymetry, gravimetric and magnetic surveys, heat flow measurements and drilling projects, an extensive assemblage of modern near-vertical and wide-angle reflection lines has been collected in the area, largely offshore, specially since the 1990s. In this study, we collect information from CSS lines available in the area resolvable with LET and incorporate it indirectly into the inversion process, aiming to preserve the strength of each method. Instead of including shots into the inversion, we rather adjust the reference model with information from CSS, which also facilitates greatly the interpretation of observed tomographic anomalies.

We present here the results of the simultaneous inversion of *Vp* and hypocentral parameters, with focus on the 3-D velocity structure of the Central Pacific margin of Costa Rica. The LET images the subducting slab as a high-velocity feature topped by a continuous band of low velocities from the trench down to ∼70 km, where the resolution of our model ends. This low-velocity band (LVB) broadens downdip and, more conspicuously, towards the east. We interpret these and other results as the outcome of slab dehydration, subduction erosion, tectonic underplating or fluid accumulation at the base of the overlying plate, and the subduction of thickened oceanic crust and accompanying bathymetric highs.

2 TECTONIC FRAMEWORK

Costa Rica is located on the western margin of the Caribbean Plate, where subduction of the Cocos Plate takes place along the MAT with a convergence direction of 32° and subduction rates varying from 8.3 cm yr^{-1} in Northwestern Costa Rica to 9.0 cm yr^{-1} in the southeast (DeMets *et al.* 1994). The high seismic activity in the area is generated by the subduction process, crustal deformation and magmatic activity along the volcanic front.

The lithosphere of the Cocos Plate subducting at the MAT today has been created at the fast-spreading East Pacific Rise (EPR) and at the present, slow-spreading Cocos-Nazca Spreading Center (CNS) and its precursors. The CNS segment has been partially modified by Galapagos hotspot magmatism. The boundary between the oceanic crusts formed at both centres is located offshore the Nicoya Peninsula (Fig. 1). The crust formed at the EPR is 24 Ma at the MAT, while the crust offshore Central and Southeastern Costa Rica has ages ranging from 19 to 15 Ma (Werner *et al*. 1999; Barckhausen *et al.* 2001), respectively. The thickness of the Cocos Plate crust varies from 5 to 7 km offshore Nicoya (Sallarès *et al.* 2001; Walther & Flueh 2002), to 6–8 km at the seamount domain (Ye *et al.* 1996; Walther 2003) and reaches up to 19–21 km beneath the Cocos Ridge (Walther 2003; Sallarès *et al.* 2003). Three domains have been identified by von Huene *et al*. (1995, 2000) in the highly variable morphotectonics displayed by the Cocos Plate offshore Costa Rica (Fig. 1). Facing the Nicoya Peninsula, the subducting seafloor has a smooth relief, whereas to the southeast the Cocos Ridge stands 2 km high over the surrounding ocean floor. The segment in between, the area of this study, stretches from the Fisher Seamount and Ridge until the Quepos Plateau, and it is 40 per cent covered by seamounts. Substantial deformation of the continental slope in the form of deep furrows and domes indicates seamount subduction and there is evidence that they remain attached to the subducting plate to depths of ∼25 km, eventually causing coastal uplift (Fisher *et al*. 1998; Gardner *et al.* 2001) and large earthquakes (Husen *et al.* 2002). The seamounts have a Galapagos geochemistry, being 13–14.5 Ma adjacent to the margin (Werner *et al.* 1999).

High-quality seismic lines, high-resolution bathymetry and ocean drilling allow the conclusion that the Middle American convergent margin has been tectonically erosive since the Middle Miocene (Ranero & von Huene 2000; von Huene *et al.* 2000; Vanucchi *et al.* 2001). Basal tectonic erosion offshore Costa Rica causes mass removal, and subsequent crustal thinning and margin subsidence, at high non-steady rates ranging from long-term ∼45 to 107–123 $km^3\ Ma^{-1}\ km^{-1}$ during the last 6.5 Ma (Vannucchi *et al.* 2003). Ranero & von Huene (2000) identified two specific mechanisms of subduction erosion along the Middle American margin: erosion by seamount tunnelling and removal of large rock lenses of a distending upper plate.

The along-strike segmentation of the Cocos Plate appears to have a strong tectonic effect on the upper plate. Significant variations in the subduction angle, the nature of the incoming plate and magmatic composition along the volcanic arc occur along this margin (Carr & Stoiber 1990; Protti *et al.* 1995a; von Huene *et al.* 2000; Husen *et al.* 2003a). In Southeastern Costa Rica, cessation of volcanic activity and accelerated uplift of the Talamanca Cordillera since 3.5 Ma have been attributed to the northwest-to-southeast shallowing of the slab as a response to the subduction of the Cocos Ridge solely or, more recently, first to the subduction of the Coiba Ridge and the passage of the Cocos–Nazca–Caribbean triple junction and the subsequent subduction of Cocos Ridge (MacMillan *et al*. 2004). This slab shallowing, together with trench retreat by forearc erosion, have been invoked to explain the northeastward migration of the volcanic front in Central Costa Rica from its position during the Miocene–Pliocene to its current location (Marshall *et al.* 2003; Fig. 1).

The basic structural configuration of the margin offshore Costa Rica and Nicaragua (Hinz *et al.* 1996; Kimura *et al.* 1997; Ranero *et al.* 2000) consists of a margin wedge composed of the same ocean igneous and associated sedimentary rocks that outcrop at several spots along the coast in Costa Rica, covered by slope sediments, underthrust by trench sediments and gouge made of upper-plate material and faced by a small frontal prism. This basic structure is altered in places where seamounts are in the first stages of subduction, but it is a short-term damage: after ∼0.5 Ma the morphology and structure of the margin become nearly undistinguishable from places were no seamount subducts (von Huene *et al.* 2000). The oceanic assemblages cropping out at the Pacific coastal areas include a pre-Campanian oceanic plateau association in the Nicoya Peninsula and in the outer Herradura Promontory; an accreted oceanic island of Maastrichtian to lower Eocene age which forms the main edifice of the Herradura Promontory; and the Quepos Promontory, formed by the accretion of an Upper Cretaceous–Paleocene seamount (Hauff *et al*. 2000; Denyer *et al.* 2006).

Coinciding with the seamount segment, the Central Pacific region of Costa Rica shows the highest seismicity rate along the southern section of the MAT. The absence of very large earthquakes ($\dot{M}_w > 7.5$) and the high rate of small earthquakes define this part of the subduction zone as seismically decoupled (Protti *et al.* 1994), while coupling increases to the northwest and to the southeast. Several studies have found evidence of the relationship between the subduction of bathymetric highs and the generation of large subduction earthquakes, like the M_w 7.0 Cóbano earthquake in 1990 (Protti *et al.* 1995b; Husen *et al.* 2002) and the M_w 6.9 Quepos earthquake in 1999 (Bilek *et al.* 2003; Fig. 1).

3 DATA

3.1 The Jacó experiment and data quality

The Jacó network, named after the coastal town were the base of operations was located, recorded more than 3000 events from April until the first days of October 2002 (Fig. 1). Around 2000 events were originated in the Central Pacific region from Costa Rica, the target area. The network recorded also the M_w 6.4 Osa earthquake from June 16 and its aftershocks, which occurred ∼30 km eastward from the Osa Peninsula (Fig. 1).

The network extended from the incoming Cocos Plate to the forearc, covering the Herradura Promontory and surroundings (Fig. 1). It consisted of 15 short-period three-component stations, equipped with Mark L4-3D seismometers and Reftek data loggers, and 23 ocean-bottom stations (OBH), with hydrophones or broad-band differential-pressure gauge sensors (Flueh & Bialas 1996; Bialas & Flueh 1999). The land stations were operated and maintained by the local Instituto Costarricense de Electricidad. Additional readings from 16 of the permanent short-period vertical-component stations of the Red Sismológica Nacional (RSN) were included in the database improving the coverage towards the volcanic front (Fig. 1). An area of 19 500 km^2 was covered with the combined array. The average station spacing for the Jacó network was 13 km, except for the area of the marine shelf where depths shallower than 200 m prevented the deployment of OBH. The station spacing in the area covered only by RSN stations is 25 km on average.

The land stations and OBH from Jacó network recorded at a sample frequency of 100 Hz. Since all stations operated for 6 months in continuous mode, the pre-processing of the raw data was laborious. A short-term-average versus a long-term average (STA/LTA) trigger algorithm was applied to search for seismic events, with the OBH data previously treated with a 5–20 Hz bandpass filter to suppress the typical long-period, marine noise.

The accuracy of the observed traveltimes depends on the accuracy of the receiver position, the precision of the internal clock of

the receiver, the sampling rate and the picking accuracy (Haslinger 1998; Husen *et al.* 2000). The Reftek instruments were equipped with GPS receivers, which provided clock synchronization and position determination every hour. By comparison between the position of one of the land stations determined by a geodetic survey and the positions reported by the GPS, the accuracy of the land station locations is estimated to be ±50 and ±20 m in the horizontal and vertical directions, respectively. The GPS time signal kept the clock drift below 8 ms. The accuracy of the OBH positions depends on the accuracy of the ship's position and on the drift during the descent of the station. By relocation of the OBH using the direct water wave from airgun shooting, their accuracy is estimated at ±250 m in the horizontal direction, while ±10 m in depth are appraised from the depth measurements conducted on board with the Simrad multibeam echosounder system and calibrated by conductivity–temperature–depth (CTD) profiling. The internal clock drift of the OBH, evaluated by its synchronization with a GPS time signal before and after recovering, is estimated to be less than 5 ms d^{-1}. Positions of most of the RSN stations have been determined by combined use of maps with scale 1:50 000 and single-point GPS measurements. The comparison between available geodetic measurements for some RSN stations outside of the study area yields the conservatively estimated position accuracy is ±300 m in longitude and latitude, and ±50 m in elevation.

Analyst-reviewed *P*- and *S*-wave arrival readings and initial locations of the events were accomplished using the program HYP (Lienert & Havskov 1995) included in the software package SEISAN (Havskov & Otemoeller 2005). We applied a weighting scheme for phase reading, with quality factors ranging from 0 corresponding to the lowest reading uncertainty (±0.05 s), to factor 4 (>0.2 s) for uncertain readings, which were not used for further modelling. Average *P*-wave reading uncertainty is estimated on ±0.07 s. The minimum 1-D model for Costa Rica, calculated by Quintero & Kissling (2001), was chosen for the initial locations since it represents an average model and deals with the fact that the data set includes earthquakes originated in different tectonic environments.

The *S*-phases from the earthquakes were picked solely from the records of the 15 Jacó land stations, which included the available three-component seismometers for the experiment. This circumstance restricts the *S*-wave coverage to the Herradura Promontory and decreases the resolution capability of the inversion for a *Vp*/*Vs* model. For that reason, only the *P*-wave modelling is presented in this work.

3.2 Controlled-source seismology (CSS) profiles in the area

In a LET of Switzerland, Husen *et al*. (2003b) successfully used the 3-D Moho topography and associated *P*-wave crustal velocities modelled by Waldhauser *et al*. (1998) from CSS profiles from all over the country as starting model. In that way, they combined both, passive and active experiment data sets in the LET while exploiting the strength and information of each. Unfortunately, although several CSS lines traverse the area of this study, they are not distributed in a network dense enough to allow for off-line migration using the interpolation scheme from Waldhauser *et al*. (1998). Nevertheless, a priori information, such as velocities and thickness of sedimentary basins, can be used to 'tune' the reference model, in this case the minimum 1-D model for the data set, adjusting the modelling in zones that cannot be resolved by LET. Moreover, the interpretation of observed tomographic anomalies is greatly facilitated by correlation with structures well resolved by near-vertical reflection techniques.

Of particular interest for the area surveyed by the Jacó experiment is the CSS profiling carried out in the Nineties by the German projects PACOMAR and TICOSECT, which aimed to explore the margin wedge and the oceanic plate structure (Hinz *et al.* 1996; Ye *et al.* 1996; Stavenhagen *et al*. 1998). We extracted information from four CSS profiles, whose location is shown in Fig. 2, to combine it with the LET: depth-migrated reflection lines SO81-06 (Ranero & von Huene 2000) and 13 (Ranero, personal communication), and wide-angle profiles SO81-200 and 100 (Ye *et al.* 1996). Profiles SO81-13 and SO81-200 are coincident. Profile SO81-100 runs parallel to the trench across the continental slope, and traverses line SO81-200. Unfortunately, the central profile from TICOSECT possesses low quality due to high-amplitude coherent noise, which caused an apparent lack of reflections from the plate boundary zone (McIntosh *et al.* 2000).

Profile SO81-200, with an average shot spacing of 150m, presents relatively good coverage and reversed observations from six OBH and two land stations distributed along 125 km. It illuminated the margin structure down to 25 km depth and was analysed by Ye *et al*. (1996) using 2-D forward modelling. For a starting model, they

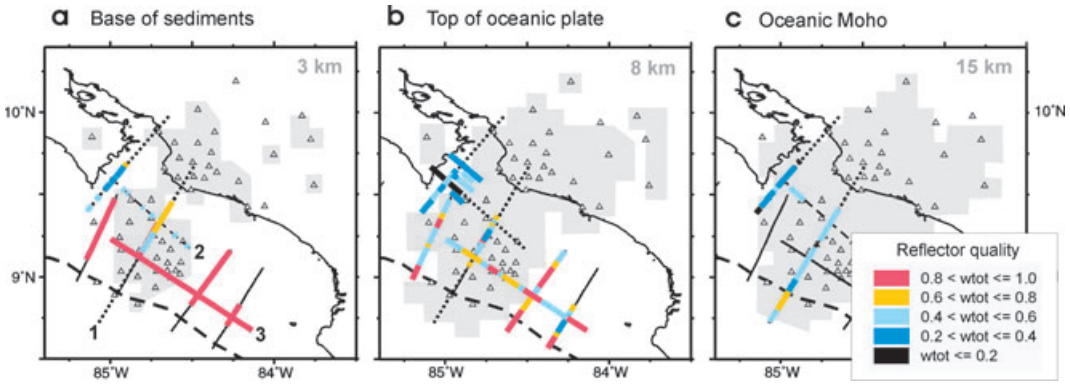

Figure 2. Controlled source seismology profiles in the study area. Dotted lines represent wide-angle profiles and continuous lines, depth-migrated near-vertical reflection profiles. Superimposed are locations of 2-D migrated reflector elements from the base of the slope sediments and the top and Moho of the oceanic plate. The inset shows the colour scale for total quality weighting factor. The grey areas indicate zones of good resolution of local earthquake tomography at 3, 8 and 15 km depth from (a) to (c), respectively. Triangles denote seismic stations of Jacó experiment, and the position of the Middle America Trench is indicated by a dashed line. 1: profiles SO81-200 and SO81-13; 2: profile SO81-100 and 3: profile SO81-06 (see text for references).

used the outline of the crustal and sedimentary structure provided by near-vertical reflection data. Wide-angle line SO81-100 included five OBH recording the shooting, but only the sedimentary layer and the top of the margin wedge were well resolved (Ye *et al.* 1996). Deeper velocities were constrained with those from line SO81-200. Prestack depth migration has been applied to the reflection lines. The iterative migration procedure uses velocities constrained with focusing analyses and common reflection point gathers. Resolution at ∼10 km is ∼0.5 km (Ranero & von Huene 2000).

Before using the information from CSS models, the reliability of the structural information needs to be assessed in terms of its uncertainty. We inspected the available CSS profiles crossing the area of this study and extracted the reflectors belonging to the slope sediments basement, known as 'rough surface' (Shipley *et al.* 1992), and to the top and the Moho of the subducting plate (Fig. 2). Quality factors were then assigned to the reflectors following the weighting scheme developed by Baumann (1994). The reflector elements from wide-angle models are weighted according to the data confidence (phase correlation, interpretation method), profile orientation in respect to the 3-D tectonic setting and profile type (reversed, unreversed). Reflector elements from near-vertical reflection profiles are ranked after the quality of their reflectivity signature, migration type (i.e. source of velocity used for migration) and projection distance. The total weighting factor ($w_{\rm tot}$) for each reflector is obtained by multiplying the individual factors.

Fig. 2 shows the location of the CSS profiles in the studied area, with the identified 2-D migrated reflectors superimposed and colour-coded according to their quality. For example, a reflector element from a wide-angle profile exhibits maximum quality ($w_{\rm tot} = 1.0$) when the phase picking is very reliable, the line is oriented along strike and the ray coverage is reversed. The reflector element from the oceanic Moho in wide-angle line SO81-200 that starts under the trench axis and stretches ∼10 km seaward received a $w_{\rm tot}$ 0.64 (Fig. 2c). This value resulted from confident phase recognition (0.8), the profile orientation perpendicular to the strike (0.8) and a good reversed ray coverage (1.0).

In general, the rough-surface reflectors from reflection lines present high $w_{\rm tot}$ values, while those from wide-angle are middle to good (Fig. 2a). Most of the reflectors from the top of the subducting plate from wide-angle profiles have weighting factors from low to middle, the values being somewhat higher from reflection lines (Fig. 2b). The latter do not provide information from the Moho; middle $w_{\rm tot}$ values are associated to the available Moho reflectors from wide-angle lines (Fig. 2c). The grey shaded areas in Fig. 2 mark the regions well resolved with our LET, according to criteria discussed later, at 3, 8 and 15 km depth, approximately the depths at which the 'rough surface' of the upper plate, and the top and Moho of the oceanic plate are expected, respectively. These are the areas were we can incorporate the CSS information into the LET, because they are resolved by both methods.

4 METHOD

4.1 Minimum 1-D velocity model

Linearization of the non-linear, coupled hypocentre-velocity problem demands initial velocities and hypocentre locations to be close to their true values. Moreover, results of LET and their reliability estimates strongly depend on the initial reference model (Kissling *et al.* 1994). We used the VELEST software (Kissling *et al.* 1995) to determine hypocentres and the minimum 1-D *P*-wave velocity model (Kissling 1988; Kissling *et al.* 1994) for the data set, that is, the velocity model and station corrections that most closely reflect the a priori information obtained by other studies, but at the same time lead to a minimum average of root mean square (rms) of traveltime residuals for all earthquakes. VELEST deals with the coupled hypocentre-velocity problem by performing several simultaneous inversions of hypocentral parameters, 1-D velocity models and station corrections.

A very high-quality subset of 261 earthquakes was selected for the derivation of the minimum 1-D *P*-wave velocity model. These events present a maximum azimuthal gap in station coverage (GAP) of 180° or less, show at least 12 *P*-wave arrival observations with the lowest reading uncertainty (±0.05 s, corresponding to weight 0) and at least one observation within a distance of 1.5 times their focal depth. Fig. 3 shows the spatial arrangement of the subset, together with the ray coverage and the hypocentre distribution in depth. A total of 4986 *P*-wave observations from 57 stations integrate the subset. As a result of geometrical considerations and the limits of the target area for the LET, we included readings from only 10 of the total RSN stations in the subset. The data set represents a fair sampling of the seismicity recorded over the period of the deployment: most of the events originated offshore, beneath the continental shelf, while fewer were generated within the subducting slab and the continental crust (Figs 1 and 3).

The ray tracer implemented in VELEST assumes that all the stations are located within the first layer of the velocity model. For the Jacó array, this implies a thickness of ∼7 km for the first layer, because the highest land station and the deepest OBH were located at 3487 and 3561 m over and below the sea level, respectively. Near-surface velocities usually exhibit a strong gradient, therefore such an unrealistic first layer with constant velocity introduces instabilities in the inversion procedure, preventing convergence. Station elevations were therefore neglected during the 1-D inversions. This exclusion implies that the resulting station corrections encompass, not only the effect of the subsurface geology and large-scale velocity heterogeneities such a dipping slab, but also of the station elevations.

Determination of the minimum 1-D model is a trial-and-error process, in which a wide range of starting velocity models are tested in order to thoroughly explore the solution space. From initial inversions with several starting velocity models with different layering (e.g. Matumoto *et al.* 1977; Ye *et al.* 1996; Quintero & Kissling 2001) we observed low velocities (<3 km s^{-1}) in the first kilometres, and strong variation at depths from 10–15 km and under 40 km. A relative good convergence was found between 15 and 40 km depth. After adjusting the layering to the depth distribution of the events in the selected subset, further trials of velocity models were conducted, including high- and low-velocity tests to investigate the dependence of the solution on the initial model. These tests confirmed that the number and distribution of hypocentres shallower than 15 km and deeper than 40 km were not favourable to resolve those layers. Since most of the events recorded by the Jacó network are located in the area where the wide-angle seismic lines SO81-100 and 200 were shot (Figs 1 and 2), the velocities for the first 15 km from the model of Ye *et al*. (1996) were adapted into the initial models and were overdamped during the inversion process. Table 1 shows the final 1-D velocity model.

The station corrections, shown in Fig. 4, display a meaningful pattern concerning the geometry of the network, distribution of earthquakes and geological setting, as well as the effect of the station elevations. The reference station was located at 160 m a.s.l. in the Herradura Promontory. The high negative delays for the OBH at the

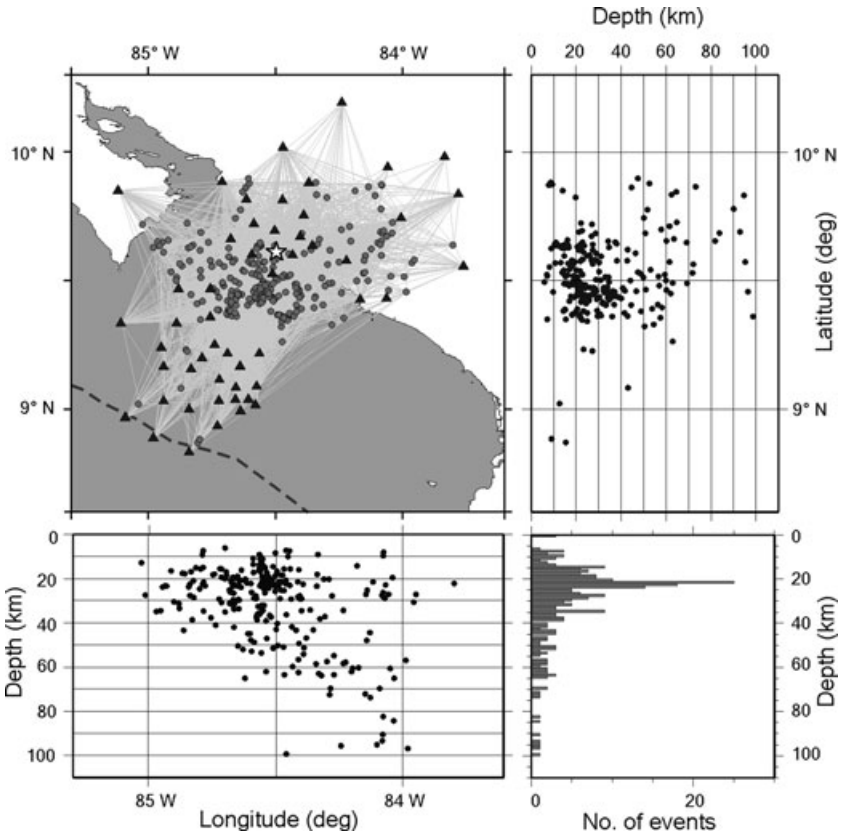

Figure 3. Distribution of 261 hypocentres selected for determination of the *P*-wave minimum 1-D model, in map view and vertical cross-sections in E–W and N–S directions. Locations estimated using the 1-D model for Costa Rica from Quintero & Kissling (2001). Only events with at least 12 *P*-wave observations and a GAP of 180° or less were used. At the lower right corner, a histogram of hypocentre-depth distribution is included. Black triangles represent stations. Grey lines show ray paths between epicentres and stations. Reference station is represented with a white star. The axis of the Middle America Trench is indicated by a dashed line.

Table 1. Minimum 1-D *P*-wave velocity model for Jacó experiment.

Depth (km)	*Vp* (km s^{-1})
0	2.50
2.5	4.90
5	5.06
7.5	5.23
10	5.50
15	6.05 ± 0.05
20	6.63 ± 0.03
25	6.95 ± 0.06
30	7.23 ± 0.08
35	7.35 ± 0.11
40	7.35 ± 0.12
50	7.50
60	7.90
80	8.20
100	8.30

southwestern end of the network compensate for the depths close to the trench and the high velocities expected from the subducting oceanic crust. A consistent positive-correction behaviour is seen for most of the OBH located over the continental slope, where low velocities (2.1–2.9 km s^{-1}) from the 2–3 km-thick slope sediments were modelled by Ye *et al*. (1996). Two OBH placed inside of a broad embayment (Fig. 4) display positive corrections lower than the rest of the stations in the continental slope. This could be attributed to the effect of their deeper locations (∼2 km). No corrections or relatively low negative corrections (<–0.4 s) resulted for onshore stations from the Jacó network, as expected from elevations and subsurface geology similar to those of the reference station. The positive delays for RSN stations located towards the volcanic front exhibit the influence of their altitude, somewhat weaker than expected, probably because of higher near-surface velocities.

The final average rms and variance for the data set are 0.129 s and 0.021 s^2, respectively, in contrast with the initial values of 0.325 s and 0.036 s^2 from the single-event mode location using the 1-D model from Quintero & Kissling (2001).

Stability tests are required for testing the robustness of the minimum 1-D model, yielding insights into the coupled hypocentre-velocity problem for the specific data set and allowing the detection of eventual outliers as well. Following Haslinger *et al*. (1999) and Husen *et al*. (1999), we conducted several tests with randomly and systematically shifted hypocentre locations. For the first series of tests, hypocentres resulting from the inversion procedure were shifted randomly up to a maximum of 10 km in any direction, and the inversions were performed both, keeping the model fixed and with a floating model. Both cases show a very good retrieval of the original hypocentre locations, indicating that they are not systematically biased and in the latter case, variations in velocities and station corrections are very close to the originals. The robustness of the minimum 1-D model was tested by systematically shifting all the hypocentres 10 km deeper, and inverting again both, with fixed and floating model. While recovery of the original hypocentre

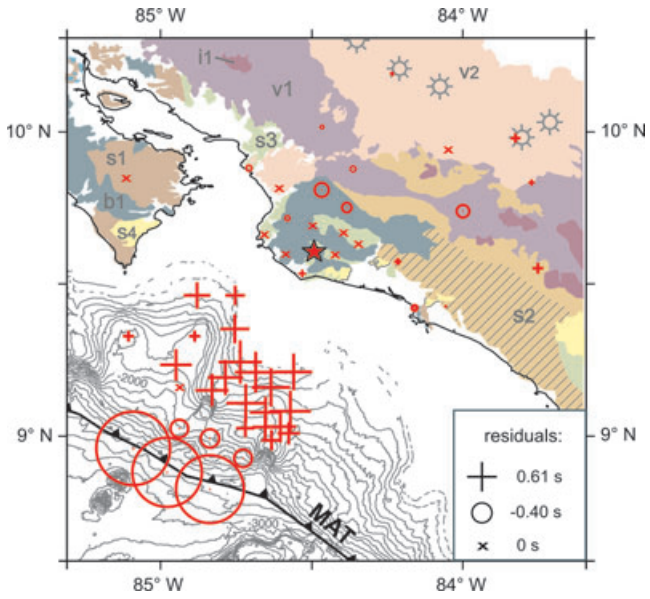

Figure 4. Final *P*-wave station corrections for the minimum 1-D model. Reference station is marked with a star. The inset indicates the sign and scale for the station corrections. Bathymetric contours every 200 m from von Huene *et al.* (2000). MAT: Middle America Trench. Geology based on Denyer & Alvarado (2007): b1: tholeiitic basalts, pre-Campanian to lower Paleogene; i1: intrusives (gabbro to granite), Miocene to Pliocene; v1: volcanism (basalt to dacite), Miocene to Pliocene; v2: volcanism (basaltic andesite), Pleistocene-Holocene; s1: turbiditic sequences, Campanian to Eocene; s2: turbiditic and subcoastal to coastal deposits, Oligocene to Miocene (hatched pattern: Térraba Formation); s3: coastal and subcoastal deposits, Miocene; s4: coastal and fluvial deposits, Plio-Pleistocene. Areas in white are Quaternary continental and coastal sediments. Radiating circles denote Holocene volcanoes in central Costa Rica.

locations in the first case is excellent, they remain close to their shifted positions in the second case. These results indicate a good degree of independence of the epicentres from the velocity structure, and a substantial coupling between the velocity and the depths/origin times.

4.2 Local earthquake tomography

We used a damped, least-squared iterative solution, the computer code SIMULPS, to solve the non-linear tomography problem (Thurber 1983; Eberhart-Phillips 1990; Evans *at al.* 1994). Hypocentre locations are treated as unknowns in the inversion as a result of the coupling of hypocentre locations and velocities. Each iteration consists of an inversion for velocities and for hypocentre locations. After each iteration, new ray paths and traveltime residuals are computed using the updated velocity model.

We chose the special version SIMULPS14, which has been modified by Haslinger (1998) to include, besides the standard approximative pseudo-bending ray tracer (ART), the full 3-D shooting ray tracer algorithm (RKP) from Virieux & Farra (1991) for the forward solution. It has been demonstrated that for ray paths longer than 60 km the RKP method yields significantly smaller errors than the ART (Haslinger & Kissling 2001).

Previous to 3-D modelling, the entire Jacó database was relocated using the minimum 1-D model with station corrections derived before. Since the coupling between hypocentre locations and seismic velocities demands a careful choosing of events used in the 3-D inversion, we selected a high-quality data set, including only events with a GAP of 180° or less and at least 8 *P*-wave arrivals. This data set encompasses 595 earthquakes with 11 310 *P*-wave observations (Fig. 5), with an average of 19 observations per event. Most of the events are located between 10 and 30 km depth, beneath the continental shelf, while the rest were generated at the Wadati-Benioff zone to depths of around 100 km, at the continental crust and at the oceanic crust close to the trench.

The first inversions revealed that neglecting station elevations during the calculation of the minimum 1-D model, as described before, caused strong coupling between hypocentres and the station corrections for the data set. For this reason, and since the locations resulting from the 1-D inversion are already close to their true values, the hypocentre parameters were kept fixed during the first iteration of the 3-D inversion, while adjustments were allowed only to the velocities. Subsequent iterations permitted updating of both, hypocentre locations and velocities.

The results and the resolution estimates, such as the diagonal element of the resolution matrix (RDE), are strongly affected by the damping parameter. The damping depends mainly on model parametrization and on the average observational error (Kissling *et al.* 2001). In this study we selected a value of 100, following the approach of Eberhart-Phillips (1986). We analysed trade-off curves between model variance and data variance (Fig. 6), constructed after two iterations applying damping parameters ranging from 1 to 10 000. The chosen damping value ensures the largest decrease in data variance without causing a strong increase in model variance, leading to the smoothest solution to fit the data. Fig. 6 also displays the trade-off curve for converged solutions, that is, when the inversion process has ended. Values lower than 100 result in a nearly constant data variance while model variance considerably increases, rendering rough models. A damping parameter of 100 also produces the data variance which more closely approaches the average weighed error of observed *P*-wave arrival picks and at the same time generates the minimum increase in model variance. It also indicates that noise is not being fit during modelling.

In SIMULPS14, the velocity model is defined at grid nodes resulting from intersecting lines in *x*-, *y*- and *z*-directions. Velocities are linear-interpolated between the grid nodes. Initial velocities for the LET were taken from the minimum 1-D model and interpolated at depth to match the gradient required by SIMULPS14 (Fig. 7). The grid spacing was selected to account for the distribution of stations and seismicity, aiming to obtain the highest possible uniformity in ray coverage and crossfiring without appealing to the use of uneven grid spacing, which complicates interpretation of results and resolution assessment (Kissling *et al.* 2001). Velocities were kept fixed at grid nodes that were not hit by any ray and, additionally, for those with a derivative weighted sum (DWS) value of less than 8.

We inverted first for a conservative horizontal grid of 15 km × 15 km and a vertical node spacing of 7.5–10 km for shallow depth (<30 km) and 20 km at greater depth. Subsequent analysis of resolution and tests with synthetic data indicated that we could use a finer horizontal grid spacing of 10 km × 10 km without decreasing the resolution quality. The distribution of the DWS, a measure of the ray density, is as homogeneous for the 15 km × 15 km as for 10 km × 10 km grid spacing, although absolute values are smaller (Fig. 8).

At this stage of the modelling we inspected the tomographic results in the light of the information provided by the CSS profiles. A first comparison of the absolute velocity distribution from the LET with profile SO81-200 (Fig. 9a) in areas well resolved by both methods revealed a fairly good agreement (Fig. 9b), considering the differences in type of data and techniques. Nevertheless, absolute

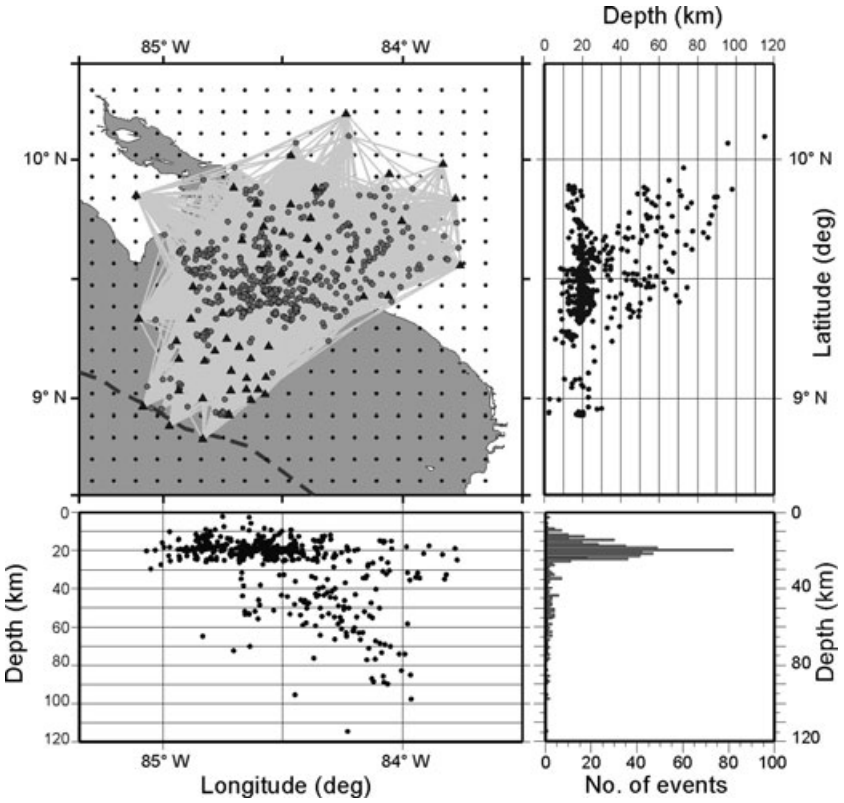

Figure 5. Hypocentre locations of 595 events selected for tomographic inversion, shown in map view and vertical cross-sections in E–W and N–S directions. At the lower right corner, a histogram of hypocentre-depth distribution is included. Black triangles represent stations. Approximate ray coverage is shown by grey lines connecting epicentres and stations. Small circles denote final, 10 km × 10 km horizontal grid-node spacing. The axis of the Middle America Trench is indicated by a dashed line.

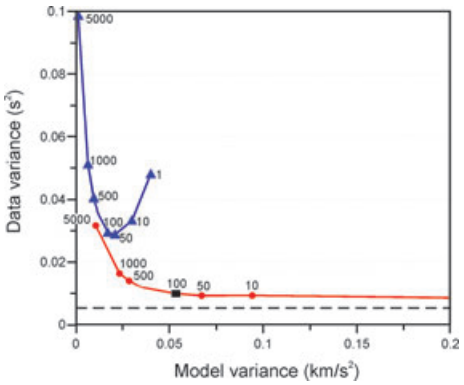

Figure 6. Trade-off curves of data versus model variance, constructed with results after two iterations (triangles) and from the converged solution (circles). Tested values of damping parameter range from 1 to 10 000 as indicated. For reasons of space and clarity, extreme values of the test are omitted. The square marks the chosen damping parameter. The dashed line represents the average weighed error of observed *P*-wave arrival picks.

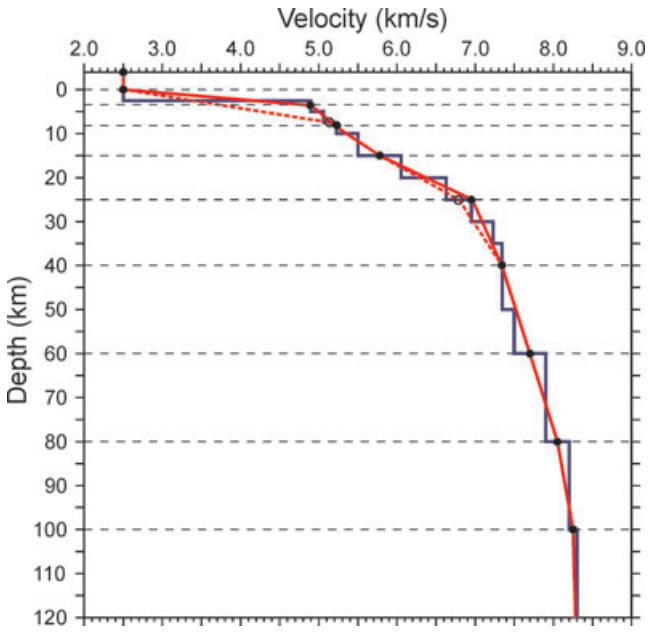

Figure 7. Velocity gradient and vertical grid nodes distribution for the 3-D inversion. The dashed line represents the original parametrization; the continuous line, the final starting model after 'tuning' with information from controlled source seismology.

velocities obtained with the LET are lower and the velocity contrasts are located deeper than in the CSS model.

Seeking to include as much information as available for the area in the 3-D inversion, and given that near-surface velocities are more reliably estimated by CSS data, we modified the original upper vertical grid spacing in order to mimic the ∼3-km-thick sedimentary coverage of the margin wedge with its corresponding velocity gradient, as shown in Fig. 7. The 3-D inversion resulted in a better match between the tomographic image and the velocity gradient given by

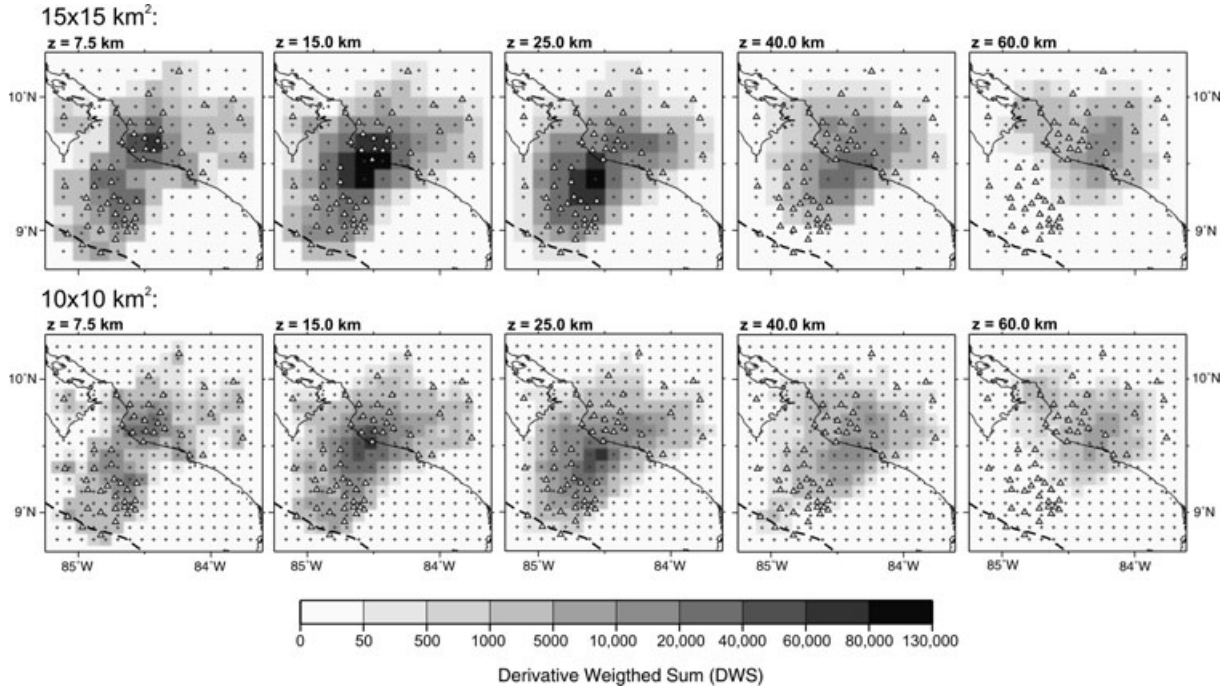

Figure 8. Derivative weighted sum (DWS) distribution in some horizontal depth sections for two different model parametrizations, as indicated. Triangles represent stations and small crosses denote grid nodes. The axis of the Middle America Trench is indicated by a dashed line.

the CSS model (Fig. 9c). Absolute velocities display a good concordance between both models in the upper oceanic crust (5.0–5.3 km s^{-1}), the continental crust (3.5–6.5 km s^{-1}) and specially in the margin wedge (3–5 km s^{-1}). Tomographic velocities in the lower oceanic crust and in the oceanic mantle, though, are very similar in both coarse and finer, 'tuned' tomographic images and remain lower than the values from wide-angle modelling at the same depths. The latter, however, are determined from unreversed observations and are thus coupled to the uncertainty in the depth of the Moho.

The subducted seamount associated with the Jacó Scar, located ∼20 km inward from the trench axis (Fig. 1), is another feature, which provides linking between the tomographic results and the CSS models. The seamount was clearly depicted as a low-velocity anomaly in the tomogram of the inversion using the coarse horizontal grid (Fig. 10a). This seamount has been displayed by reflection lines SO81-06 and 13 (von Huene *et al.* 2000), which cross each other, and by gravimetric modelling (Barckhausen *et al.* 1998), in an area where its presence was previously suspected from images of high-resolution bathymetry: a portion of the margin slope is disrupted, showing a doming in the middle continental slope and a scar left by the failure of the slope sediments (von Huene *et al.* 1995, 2000). Nevertheless, reducing the horizontal grid spacing to 10 km × 10 km and introducing a closer vertical spacing in the upper 10 km had a negative effect on the definition of the seamount image, as shown in Fig. 10(b). This loss indicates a decrease in the resolution capability in this area due to limited ray coverage. Moreover, introducing grid nodes at 3 km depth with higher velocities than in the original inversion modifies ray paths and reduces the velocity gradient between 5 and 10 km depth, resulting in a weaker contrast of the low-velocity anomaly at those depths. In a good example of the significance of parametrization in tomography, particularly when studying velocity structure details, we were able to improve the seamount image in the finer grid by slightly shifting (∼6 km to the southwest) the location of the fine grid nodes so that a grid node coincides with the seamount position as estimated by CSS lines and the coarse LET (Fig. 10c).

The final tomographic model achieved a data variance reduction of 66 per cent compared to the 1-D reference model. The final weighted rms over all traveltime residuals is 0.083 s. This value is close to the a priori observational error, indicating convergence of the inversion.

4.3 Solution quality

The heterogeneous arrangement of sources and receivers in a LET limits the area of good resolution and may lead to the introduction of artefacts. In general, the solution quality of a certain volume depends mainly on the geometrical distribution and density of rays. Classical tools to asses ray coverage include the display of resolution estimates such as hit count, derivative weighted sum (Fig. 8), diagonal elements of the resolution matrix (RDE), and the spread function (see e.g. Reyners *et al.* 1999; Husen *et al.* 2000). Tests with synthetic data are a powerful tool, not only to gain useful information about model parametrization and damping, but to define areas of good and low resolution (Kissling *et al.* 2001). These tests consist of the construction of synthetic input velocity models and the computation of synthetic traveltimes using the same source–receiver distribution of the real data set, and of inversion applying identical model parametrization, damping, and number of iterations as for the real data.

We undertook at first two types of synthetic tests, checkerboard and characteristic models (Haslinger & Kissling 2001) and, considering the results of the inversion of real data, we further designed a synthetic model to test for slab structure. The synthetic traveltimes through the models were calculated using the finite-difference technique of Podvin & Lecomte (1991). Gaussian-distributed noise proportional to the original observational uncertainty was added to the traveltimes.

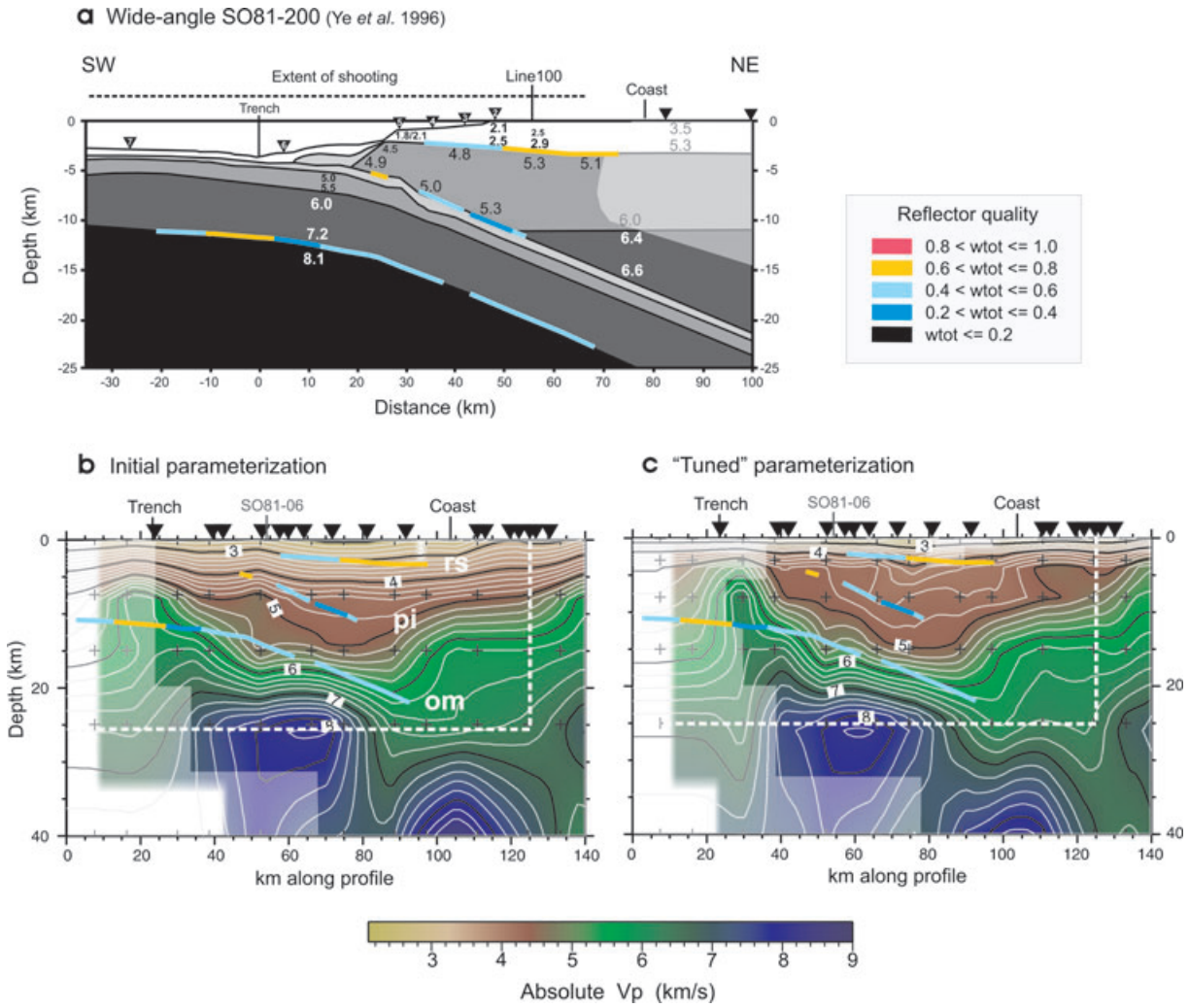

Figure 9. Comparison between wide-angle profile SO81-200 model (Ye *et al.* 1996) and local earthquake tomography results. Cross-sections (b) and (c) display absolute velocity tomograms coincident with profile SO81-200, using initial and 'tuned' parametrization (see text for description), respectively and including reflectors from the sediment cover (rs), the top of the slab (pi) and the oceanic Moho (om) from that profile, as indicated. Areas of lesser resolution are masked. Colour code for reflector quality as in Fig. 2. Profile location is given in Fig. 2. Dashed line in (b) and (c) marks the area modelled by profile SO81-200. Inverted triangles represent stations.

We performed synthetic checkerboard tests in order to explore the regions of the model where it is possible to resolve small-scale structures (see Fig. S1). Following Husen *et al*. (2004), two checkerboard models were designed, each consisting of alternating high- and low-velocity anomalies (±10 per cent) with one grid node left open in between to test for horizontal smearing; at the same time, every other layer is free of anomalies to test for vertical smearing. One model has anomalies placed at 0, 8, 25 and 60 km depth, and the other at 3, 15, 40 and 80 km depth. The tests were conducted for anomalies spanning over two grid nodes in *x*- and *y*-direction (Fig. S1a), and repeated for anomalies encompassing just one grid node (Fig. S1b). As an example, Fig. 11 presents only the results from the checkerboard tests using the second model and one-grid node anomalies. The resolution is very good both off and onshore, even at depths greater than 40 km and with one-grid anomalies. As expected from the earthquake distribution (Fig. 5), at 60 km depth resolution is still good onshore, also for the model with one-grid anomalies. Vertical smearing is low at all depths, but it is slightly stronger in the first 8 km. Starting at 25 km depth, some minor horizontal smearing oriented northeast–southwest is detected offshore. Amplitude recovery is also good, reducing to a more moderate ability between 40 and 60 km depth.

Since checkerboard tests cannot ensure that the data set is able to resolve larger scale structures (Leveque *et al.* 1993), following Haslinger *et al*. (1999) and Husen *et al*. (2000) we designed an input characteristic model, based on the inversion results obtained with the real data set (see Fig. S2). This synthetic model retains the sizes and amplitudes of anomalies seen in the tomographic images but with rotated shapes and different signs. Areas of good resolution are those, which show a good recovery of the synthetic model. In agreement with the checkerboard tests, we observe that the central part of the modelled area is well resolved down to depths of 60 km, with resolution decreasing with depth. Horizontally, the well-resolved area extends from the trench, until 25 km depth, to the volcanic front. The area resolved at 40 and 60 km depth is broader to the southeast because the deeper earthquakes used for the tomography occur closer to the trench there. A very good recovery of boundaries between high- and low-velocity anomalies is observed. Amplitude restitution is excellent from 3 to 25 km depth, although at levels shallower than 10 km the recovery is patchy. At

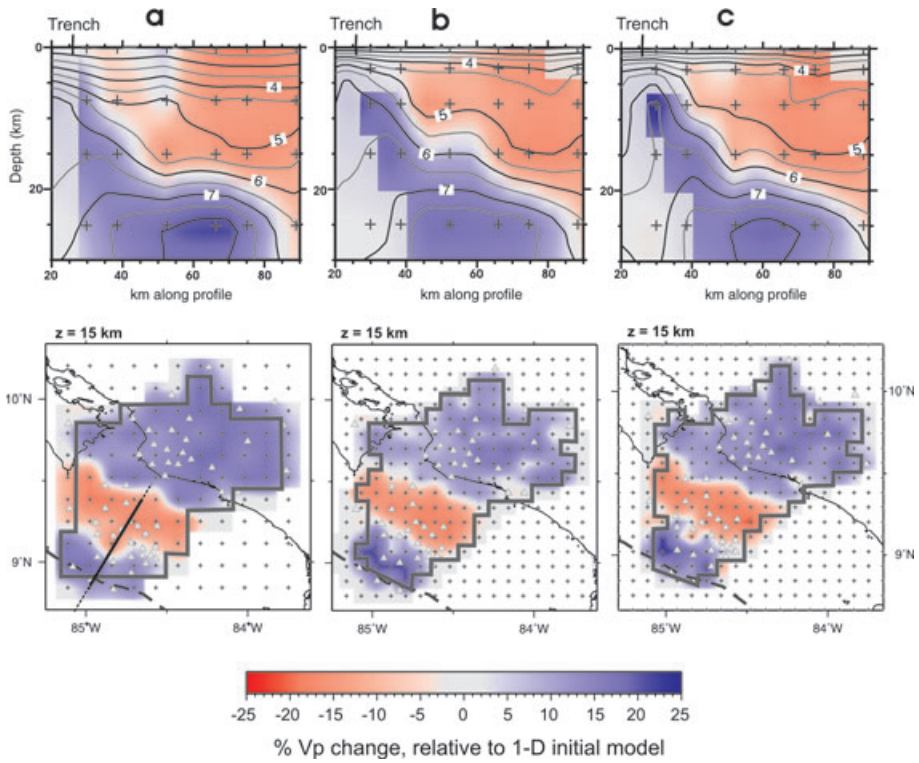

Figure 10. Effects of different model parametrizations on the tomographic image of Jacó seamount. Cross-section (as indicated) and depth slice from: (a) coarse horizontal grid of 15 km × 15 km; (b) horizontal grid 10 km × 10 km, tuned vertical grid; (c) horizontal grid 10 km × 10 km, tuned vertical grid and slight shifting of the coordinates origin of the horizontal grid. Grey lines encompass well-resolved areas as indicated by different resolution tests (see text for details). Triangles represent stations, and the dashed line the Middle America Trench. See text for discussion.

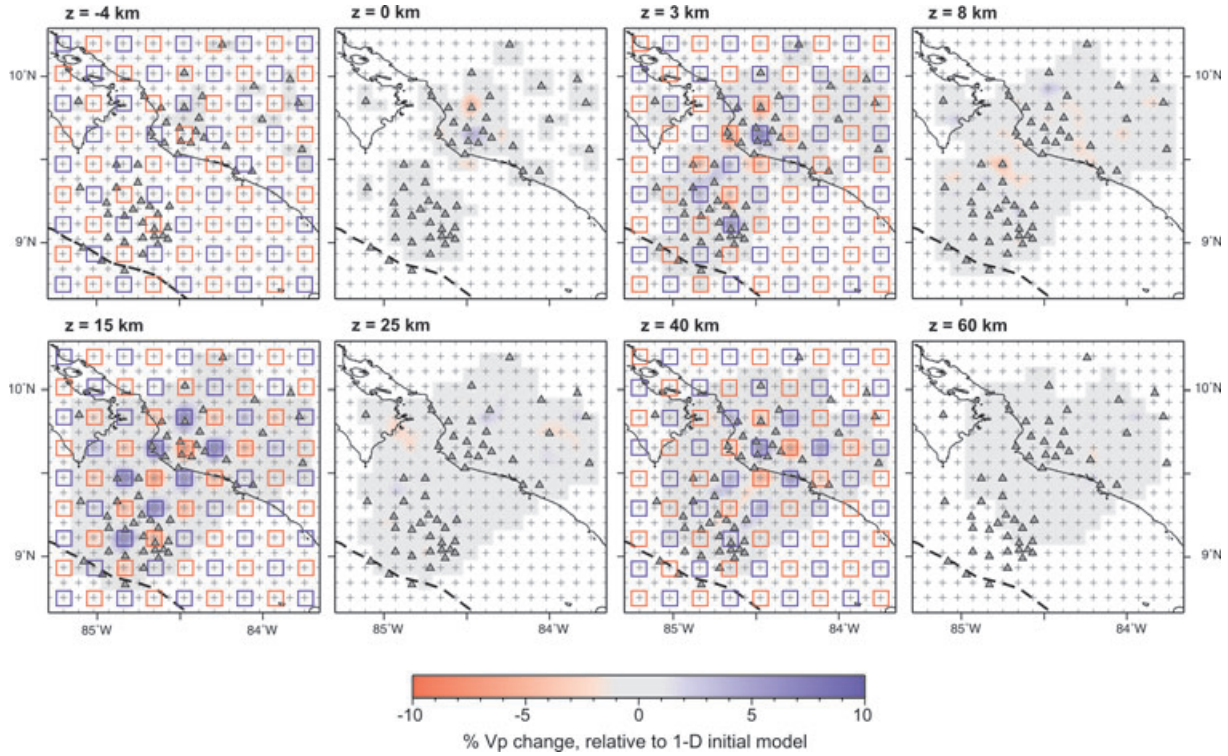

Figure 11. Horizontal depth sections with assessment of solution quality using synthetic checkerboard models. Recovered model is shown in plane views at different depths, as an example of the checker models with one-grid sized anomalies (see text for explanation). Locations of high (+10 per cent) and low (–10 per cent) velocity input anomalies are shown by blue and red squares, respectively. Small crosses represent grid nodes of the model parametrization, grey triangles denote seismic stations. The axis of the Middle America Trench is indicated by a dashed line.

40 km depth the amplitudes are more reduced, ranging from ∼60 to 80 per cent, and at 60 km and deeper, recovery is ∼60 per cent. Some horizontal smearing is observed offshore again at 40 km depth, probably caused by the fact that earthquake hypocentres deeper than 30 km are found towards the volcanic front, generating ray paths to the OBH oriented mostly northeast–southwest.

We examined also values and pattern of the RDE and the resolution contours (see Fig. S2), which help to visualize the orientation and spatial bias of possible velocity smearing in 2-D, that is, the dependency of the solution of one model parameter on its neighbours (Reyners *et al.* 1999). An excellent correspondence is observed between areas considered as well resolved according to the characteristic model test and the RDE values, and the areas outlined by resolution contours where the off-diagonal elements of the resolution matrix are still 70 per cent of the corresponding diagonal element. The RDE values of the model range from 0.01 to 0.73; most are between 0.05 and 0.40. These values are the result of the model parametrization and the damping, both conservatively chosen. Additionally, comparison with areas qualified as well resolved by the characteristic-model test yields a cut RDE value of 0.04 for good resolution. As indicated by the resolution contours, significant smearing for depths greater than 3 km occurs only at model parameters located at the edges of the volume.

As seen partially in Fig. 10 and described later in the results section, from the trench down to 60–70 km depth the tomographic images illuminate the general configuration of the margin as a high-velocity subducting slab with a band of low velocities on top. In order to test the ability of the data to resolve this structure, we calculated synthetic traveltimes through a model consisting of a high-velocity slab (+15 per cent) overlain by a relatively thin band of low velocities (–10 per cent), displayed in Fig. 12(a). Between 15 and 65 km depth, the vertical grid spacing of this synthetic model is 10 km, which is closer than the parametrization of the real model, making it more realistic. A thickening of the LVB towards the east mimics the results obtained using the real data. Modelling using the same inversion parameters determined for the real data set gave the

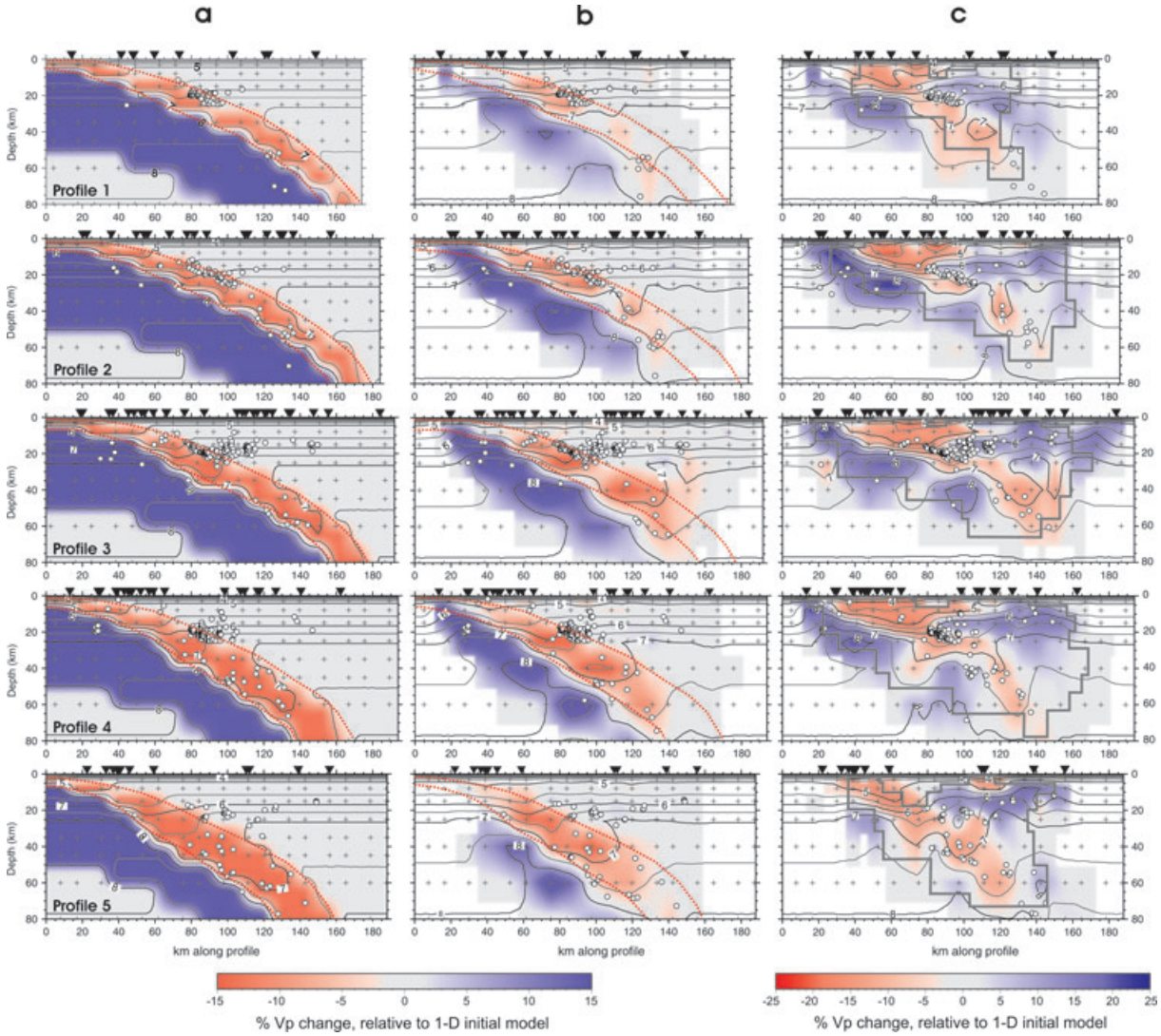

Figure 12. Synthetic test to examine the ability of the data to solve the observed slab structure. Column (a) shows the model used to derive synthetic traveltimes, while column (b) displays the results of their inversion. For comparison, column (c) presents the tomograms using the real data. Cross-sections show velocity structure as percentage change relative to the minimum 1-D model derived in this study; contours correspond with absolute velocities. Location of the cross-sections is given in Fig. 1. Earthquakes located within 8 km of either side are projected onto the profiles (white circles). Inverted triangles represent stations and small crosses denote grid nodes. Dotted red lines delineating the band of low velocities are added to ease comparison.

results presented in Fig. 12(b). Column (c) in Fig. 12, showing the results with real data along the same profiles, has been added to ease comparison and discussion.

Fig. 12(b) shows that, although decreased towards the borders, the amplitude recovery of the model is very good along the studied portion of the margin. In the centre of the model (profiles 2–4), the high velocities of the slab are well recovered from the trench down to 40 km depth. Amplitudes are slightly decreased below that depth but the continuity of the slab is still clearly displayed. At the edges of the model volume (profiles 1 and 5), amplitudes are significantly reduced, but the slab still appears as a continuous feature. Comparison of amplitude restitution from profiles 1 to 5 indicates a lateral change in resolution from northwest to southeast, with mainly the upper or the lower part of the volume well resolved, respectively. The band of low velocities on top of the subducting slab is well recovered between 15 and 25 km depth along all profiles. At 40 km depth low velocities are well recovered along profiles 3–5, where it appears as a continuous band. Between kilometres 130 and 150 along profile 3 there is a leakage of low velocities from the slab into the overlying forearc mantle, caused by rays travelling through the slab and upward towards the stations located onshore. In summary, the tests revealed that we can reliably image a low-velocity zone and its eastward thickening on top of a high-velocity slab throughout our model. An additional test using a synthetic model with a thin, uniform LVB showed equally good recovery, increasing our confidence in the capability of the data to reproduce a real feature (see Fig. S3).

5 RESULTS

The tomographic results are presented in several depth slices (Fig. 13) and vertical depth sections perpendicular to the trench (Fig. 14), whose locations are shown in Fig. 1. Depth sections show *Vp* in relative and absolute values. The indicated areas of good resolution have been defined following the previous discussion on the solution quality. In general, the tomographic model has a good resolution from the trench to the southwestern flank of the volcanic front, varying in the vertical direction down to depths of 60–70 km in the northwest and central parts of the area, and of 80 km in the southeast. We describe the results by regions, referring to the east, central and west zones of the studied area, which along the coast correspond to the entrance of the Nicoya Gulf, the Herradura Promontory and the Parrita lowland, respectively (Figs 1 and 13).

In an attempt to define the top of the subducting plate, as shown in Fig. 14, we consider the position and depth of the trench axis (3.3–3.7 km), absolute velocity values and velocity perturbations, as well as the distribution of the intraslab and interplate seismicity, which forms a clear dipping planar feature (Figs 12 and 14). The model of Ye *et al*. (1996) for profile SO81-200 predicts velocities in the upper oceanic crust between 5.0 and 5.5 km s^{-1} (Fig. 9a). Applying those values as a guide in our model renders coherent results with the interplate seismicity for the first 15 km. At greater depths we use the clear contrasts between high- and low-velocity anomalies, and the distribution of the intraslab seismicity.

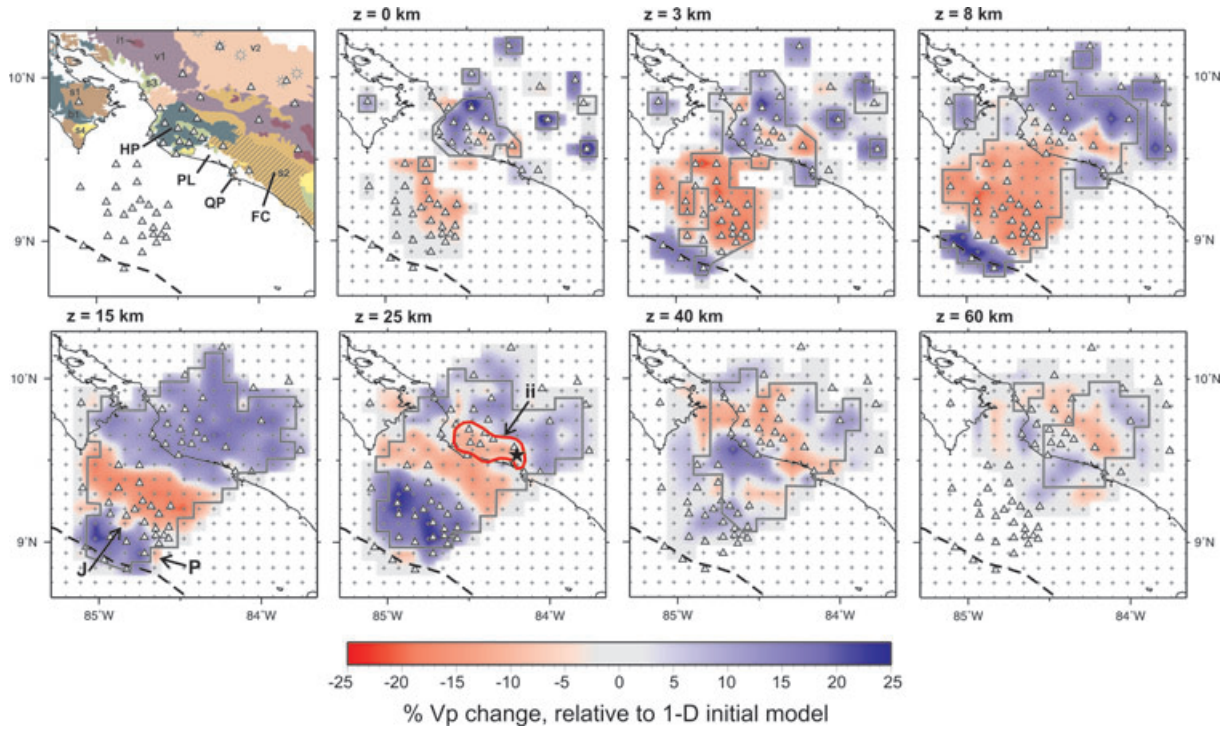

Figure 13. Tomographic results of 3-D *P*-wave velocity model shown at different depths. Velocity perturbations relative to the minimum 1-D model are shown with red to blue colours, for velocities lower and higher than predicted by the minimum 1-D model derived in this study, respectively. Areas with no ray coverage are masked. Dark grey lines contour areas of RDE > 0.04 (see text for discussion). At 25 km depth, red lines contour the low-velocity anomaly ii, observed below the inner forearc (see text for discussion) and the star, the epicentre of the 2004 M_w 6.4 earthquake (Pacheco *et al.* 2006). Triangles represent stations and small crosses denote grid nodes. The axis of the Middle America Trench is indicated by a dashed line. HP: Herradura Promontory, QP: Quepos Promontory, PL: Parrita lowland, FC: Fila Costeña (hatched pattern), J: Jacó seamount and P: Parrita seamount. Geology as indicated in Fig. 4.

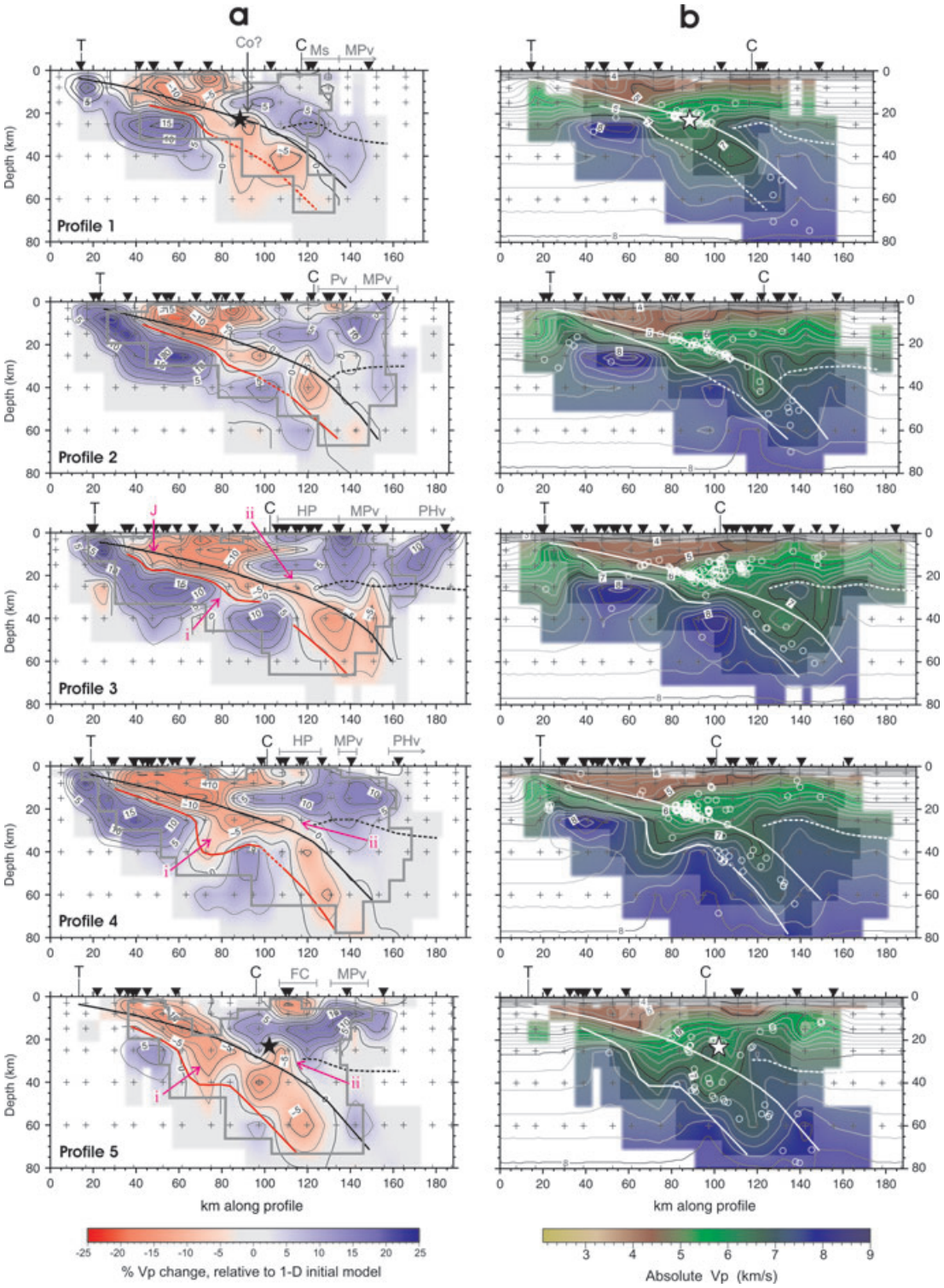

Figure 14. Vertical depth sections along the Central Pacific margin off Costa Rica showing the 3-D *P*-wave velocity structure. Location of profiles are indicated with dashed lines in Fig. 1. Column (a) shows velocity structure as percentage change relative to the minimum 1-D model; grey lines contour areas of RDE > 0.04 (see text for discussion). Column (b) presents absolute velocities; areas of good resolution are shown in full colours, areas of lesser resolution in faded tones. Earthquakes located within 8 km of either side are projected onto the profiles (open circles). Inverted triangles represent stations and small crosses denote grid nodes. Bold lines indicate the position of the plate interface and the continental Moho (dotted) as interpreted in this study (see text). The bottom of the low-velocity band (LVB) on top of the slab (see text for explanation) is delineated by red (column a) and white (column b) lines, dashed over artefacts interpreted from test for slab structure (Fig. 12). Anomalies i and ii as indicated in the text. Stars represent 1990 M_w 7.0 (profile 1) and 2004 M_w 6.4 (profile 5) earthquakes, from Husen *et al.* (2002) and Pacheco *et al.* (2006), respectively. T and C represent the trench and coast locations, respectively. HP: Herradura Promontory, FC: Fila Costeña (Coastal Range), Ms: Miocene coastal deposits, MPv: Miocene–Pliocene magmatic front, Pv: Pleistocene volcanism, PHv: Holocene volcanic front, Co: Cóbano seamount and J: Jacó seamount.

5.1 Near-surface geology

Although the resolution at sea level is restricted to relative small areas and some velocity smearing has been detected, several clear anomalies there and at 3 km depth reflect very well the near-surface geology (Figs 4 and 13). The oceanic-assemblage formations cropping out along the coast appear as high-velocity anomalies at Nicoya Peninsula and the Herradura and Quepos promontories, with absolute values between 3.0 and 5.4 km s^{-1}. The Pleistocene debris-flows (alluvial) deposits that outcrop northwestward from Herradura and the underlying Miocene coastal sedimentary rocks (Fig. 4) are congruously imaged as a low-velocity anomaly. The Pleistocene volcanic front and the volcanic formations from a previous, Miocene–Pliocene magmatic front located closer to the coast represent high-velocity perturbations. The extensive negative anomaly expanding from the trench towards the coast with velocities from 3.8–4.6 km s^{-1} could be related to both, the upper part of the margin wedge and the up to 3-km thick sediment coverage revealed by reflection profile SO81-13 (von Huene *et al.* 2000). The subducting plate appears at 3 km depth at the trench as a high-velocity anomaly, with maximum absolute velocities of 5.6 km s^{-1}.

From the surface down to 8 km depth a low-velocity anomaly with absolute velocities of 4–5 km s^{-1} has been imaged beneath the Parrita lowland, between Herradura and Quepos (Fig. 13 and Fig. 14, profile 5) but possibly extending further to the southeast, outside of the model. The projection of the anomaly onto the surface coincides very well with the northeasternmost outcrops of the dense sequences of Oligocene turbidites from the Térraba Formation (Figs 4 and 13) which constitute the main part of the Fila Costeña (Coastal Range), an inverted forearc basin thought to have been exhumed as a response to the subduction of the Cocos Ridge (Corrigan *et al.* 1990). To the northwest and north, the perturbation ends sharply against a high-velocity body, possibly related to the Miocene volcanic front. The northwest end follows the strike of the Parrita fault (Marshall *et al.* 2000; Denyer & Alvarado 2007), which limits the Herradura Block (Fig. 4). This fault is part of an active system oriented at high angles to the margin. This system separates forearc blocks with different uplift rates, interpreted as a response to subduction of seafloor roughness (Fisher *et al.* 1998; Marshall *et al.* 2000). Seaward, the low-velocity perturbation is limited by the positive anomaly under Quepos Promontory (Fig. 13). Stavenhagen *et al*. (1998) report that the Térraba Basin consists of intermediate velocity sediments (3.0 km s^{-1}) and to have a thickness of 2 km; Rivier (1985) estimates 3.5 km thickness on the basis of gravimetric models. The low-velocity zone of our model extends down to 8 km depth, where a down bending of the 5 km s^{-1} contour is found, but some amount of vertical smearing could slightly enlarge the image.

5.2 Subducting slab

The portion of the slab resolved by this study shows dipping angles of 10°–12° from the trench down to 15 km depth. The dip increases to 16°–25° at the seismogenic zone, from 15 to 25 km depth, and steepens further towards the east (Fig. 14, profiles 4 and 5). Deeper than 40 km the slab dips at 40°–45°.

The west and central zones of the margin display basically a similar velocity structure (Fig. 14, profiles 1–3), although we observe some medium-scale variations. From the Nicoya Gulf entrance to the eastern flank of the Herradura Promontory, and from the trench downward to depths greater than 60 km, the Cocos Plate is imaged as a high-velocity body with a LVB on top. The intraslab seismicity deeper than ∼30 km takes place in this band. The LVB has been delineated in the profiles in Fig. 14. Down to 20 km depth, velocity changes up to –12 per cent in the upper part of the slab; at greater profundity, maximal observed changes are of –5 per cent. The latter value could actually reach –8 per cent, taking into account that the model capacity to recover amplitudes diminishes at levels deeper than 40 km, as indicated by the synthetic tests (e.g. Figs 11 and 12). The absolute velocity along the top of the slab is 5 km s^{-1} down to 15 km depth; from 15 to ∼25 km depth the velocity gradient increases to reach 7 km s^{-1}, a value that persists almost constant down to 40–45 km depth. Velocities of 7.4 km s^{-1} appear along the top of the slab at ∼40 km depth in the west but at 50–55 km depth towards the centre.

The LVB is interrupted by high velocities at around 35–40 km depth, between kilometres 90–110 along cross-sections 2–5 (Fig. 14). The results of the test for slab structure (Fig. 12) discussed above indicate that this gap in the LVB is an artefact only in profile 2. From the trench down to 25 km depth, the LVB encompasses the first 5–7 km of the slab. At 25 km depth and 50–60 km from the trench, the tomographic images show a down bending of the 0 per cent *Vp*-anomaly contour, indicating an increase in the thickness of the LVB. In cross-sections 1–2 (Fig. 14) the thickness of the LVB increases to 10–12 km. Starting at profile 3, a pronounced down bending of the lower part of the LVB, marked as anomaly i in Fig. 14, is found along 30–40 km and between 25 and 40 km depth, specially conspicuous in cross-section 4. Absolute velocities in this anomaly range from 6 to 7.2 km s^{-1}. The LVB widens strongly downdip of this sharp contortion, encompassing more than 15 km. Neither the resolution contour maps nor the results from the test for slab structure (Fig. 12) show vertical velocity leakage or artefacts along this portion of the cross-sections. Furthermore, inversions of the real data set using a closer vertical grid-node spacing (10 km) from 25 to 45 km depth yielded identical results, ruling out the possibility of the widening being caused by a change in the grid-node spacing.

Thus, in the east zone, coinciding with the upraise of the Fila Costeña onshore (Fig. 13), the margin structure changes considerably over a distance of only ∼15 km (Fig. 14, profile 5). Besides the presence of anomaly i, the top of the slab presents here a more uniform absolute velocity gradient in the first 30 km in depth, and the LVB is notably wider at depths larger than that, comprising up to 20 km. The existence of a wider LVB in this area is confirmed by the results from the test for slab structure, which demonstrates that a high-velocity slab could be resolved (Fig. 12), even if the amplitude recovery is not optimal. Velocities of 5 km s^{-1} along the top of the slab are found down to 10–15 km depth; the 7 km s^{-1} contour appears between 30 and 35 km depth. Velocities of 7.4 km s^{-1} at 45 km and of 7.8 km s^{-1} at 65 km depth are probably overestimated, since amplitude recovery of the model decreases for depths greater than 40 km and in general towards the east (Fig. 12).

The reflection line SO81-06 reveals that the Jacó seamount has ∼25 km diameter and its summit, according to the depth migration, is located at 5 km depth (Fig. 9). The tomographic image of the seamount (Fig. 10 and Fig. 14, profile 3) coincides in horizontal extend with the reflection data, appearing as a low-velocity anomaly down to 15 km depth and suggesting thickening of the oceanic crust. We observe an up bending of the contours slower than 5 km s^{-1}, although the upper part of the seamount is difficult to define because of the similar velocities found in the overlying margin wedge. Some minor vertical velocity smearing is indicated at 8 km depth by resolution contours. Velocities higher than 5 km s^{-1} show a down bending even at 20 km depth (Fig. 14, profile 3). To the southeast

of Jacó seamount, another seamount of similar size, closer to the trench and related to the Parrita scar on the continental slope, has been imaged outside of the area of fair resolution (Fig. 13, 15 km depth).

5.3 Margin wedge and continental crust

The east and central zones show a pronounced low-velocity anomaly in the upper plate that starts some kilometres from the trench axis and extends from the surface down to the plate interface, to a depth of ∼20 km (Fig. 14, profiles 1–4). Its lower limit shallows towards the coast and finishes at ∼75 and ∼85 km from the trench axis in the west and central parts, respectively. The velocity changes up to –10 per cent, with some spots reaching –15 per cent (Fig. 14, profiles 2–3). The absolute velocities in this anomaly vary from 3.5 to 6.0 km s^{-1}. We identify this low-velocity zone as the margin wedge, with base on results from wide-angle profiles, which present a similar velocity distribution. Low velocities are justified by the normal faulting in the margin wedge across the middle slope revealed by high-resolution seismic records (Hinz *et al.* 1996; Ranero & von Huene 2000). Moreover, local fluid venting form the plate interface takes place through these faults (Hensen *et al.* 2004). Although the uppermost 10 km do not present the best resolution between the continental slope and the coast in the east zone, the area of the margin wedge seems to narrow again, extending up to 65 km from the trench axis (Fig. 14, profile 5).

Landward, the margin wedge is laterally limited by a positive anomaly representing the continental crust. It extends down to 30–35 km depth, where absolute velocities range from 3.0 to 7.0–7.2 km s^{-1}. The velocity gradient decreases at depths greater than 10–15 km, a change roughly marked by the 6 km s^{-1} contour. The most conspicuous high-velocity anomalies, with more than 15 per cent velocity change, are located in the upper crust beneath the southwestward edge of the Miocene volcanic arc (Fig. 14, profiles 3–5).

The high velocities of the upper plate are interrupted beneath the inner forearc by a low-velocity anomaly, termed anomaly ii in Figs 13 and 14. The anomaly coincides spatially with the appearance of anomaly i and the thickened LVB on top of the slab (Fig. 14). Anomaly ii roughly emerges at the downdip end of the interplate seismicity and seems to be itself aseismic. It extends from 25 km down to 35–40 km depth, where it joins the slab top, following the coastline from beneath the west part of the Herradura Promontory until Quepos, and stretching ∼20 km landward. Absolute velocities within the anomaly are 6.5–6.8 km s^{-1}. Underneath the Parrita lowland, anomaly ii increases in amplitude and shows a more conspicuous shape in cross-section (Fig. 14, profile 5). Eastward from Quepos Promontory the perturbation seems to disappear, although we reach there the limits of the volume illuminated by our data set (Fig. 13, 25 km depth). In their LET for Costa Rica, Husen *et al*. (2003a) also imaged this low-velocity anomaly and proposed that it could be caused by the presence of a subducted seamount.

5.4 Continental Moho and forearc mantle wedge

Previous works in Costa Rica determined depths between 30 and 43 km for the Moho discontinuity, and reported that the velocity contrast between the mantle and the crust is weak (Matumoto *et al.* 1977; Quintero & Kulhánek 1998; Quintero & Kissling 2001; Sallarès *et al.* 2001; DeShon & Schwartz 2004). Wide-angle profiles in the Central Pacific area (Ye *et al.* 1996; Stavenhagen *et al.* 1998) did not illuminate depths greater than ∼20 km. DeShon *et al.* (2006) inferred the continental Moho location under Nicoya Peninsula following a turnover of the contour for *P*-wave velocities of 7.0–7.2 km s^{-1}, which they found to be in good correspondence with lower crust velocities from the refraction model of Sallarès *et al*. (2001). Our tomographic results show an increased velocity gradient together with a clear bending of the 7.0–7.2 km s^{-1} contours, supporting DeShon *et al*. (2006) assumption. We observe a sharper velocity gradient in the western and central parts of the area (Fig. 14, profiles 1–3), becoming more diffuse towards the east (Fig. 14, profiles 4–5). Beneath the coast and landward, the Moho appears at 30–35 km depth (Fig. 14, profile 5). The forearc mantle wedge exhibits velocities of 7.2–7.6 km s^{-1} in the east and the west. In the central part, slower velocities of 6.8–7.2 km s^{-1} are modelled (Fig. 14, profile 3), but they are most likely caused by upward velocity leakage from the LVZ, as indicated by the test for slab structure (Fig. 12).

6 DISCUSSION

In this study, we collected information from CSS lines available in the area resolvable with LET and incorporate it indirectly into the inversion process. Usually, when CSS data are inverted directly in a LET, shots are treated as earthquakes with known origin time and location, and therefore they are not relocated during the inversion process. However, the location of the sources at the surface can negatively affect the inversion because of the stronger non-linearity resulting from the dependence of the ray turning points on the velocity structure (Laigle & Hirn 1999). Shots recorded along a seismic refraction line densely sample the wavefield in a specific direction and represent a powerful tool to obtain a model of the underlying structure, with velocities averaged along the ray paths. The data quality is often very different for CSS and earthquake data sets. Due to a better phase correlation, refraction data can often be picked with higher accuracy than LET data. Kissling *et al*. (1995) point out that data from experiments so different should not be mixed and treated in a similar way by a trial-and-error process that involves many inversions; rather, the data should both be used in different ways that exploit their strengths.

A good agreement is observed between the distribution of absolute velocities of the 'tuned' tomography and the 2-D model of Ye *et al*. (1996) for wide-angle profile SO81-200, although the velocity contrasts appear 2–5 km deeper in the tomograms (Fig. 9). This could be attributed to the differences in the estimation of velocities of each method, as well as their inherent uncertainties. While LET yields a volume-wise average of velocity, wide-angle 2-D ray tracing modelling averages velocities along the ray path. The earthquake distribution in 3-D ensures precise information of seismic velocities per volume, provided that there are enough rays per volume, coming from different directions. Also, the location of both, sources and receivers outside the studied area restricts the ability of CSS methods to resolve the precise position and true dip of reflecting structural elements. The strength of the wide-angle method lies in its sensibility to large-scale vertical and horizontal velocity gradients and discontinuities. Ray crossfiring is limited in 2-D CSS profiles, and the velocities resulting from ray tracing and in-line migration are averages for the specific layers. On the other hand, LET resolution capability is limited by the grid-node spacing, therefore decreasing with depth.

Ye *et al*. (1996) do not discuss the uncertainties of their model for the wide-angle line SO81-200, but they do mention that the

denser station coverage over the continental slope and the recordings from two land stations allowed them to determine the velocity distribution more reliably there. These authors also state that their data did not suffice to resolve the change in the velocities of the oceanic crust farther landward. A very rough estimation of the vertical uncertainty could be attempted on the basis of Fresnel volumes and the w_{tot} of reflector elements. A reflector element from profile SO81-200 with the highest quality ($w_{tot} = 1$), belonging to the plate interface beneath the margin wedge, at ∼10 km depth, would have an uncertainty of ±1.4 km considering a seismic frequency-content range of 6–14 Hz (Ye *et al.* 1996) and an average velocity of 4.3 km s^{-1} for the overlying crust. As suggested by Baumann (1994), dividing that value by the actual w_{tot} of the reflector, 0.5 in this example (Figs 2 and 9), yields ±2.8 km as an estimate of the real vertical uncertainty for the element. An example of uncertainties in wide-angle modelling is given by Walther (2003), who analysed a profile shot over the Cocos Plate, parallel to the MAT, from Quepos Plateau to the southeastern flank of the Cocos Ridge. He applied conventional 2-D ray tracing and an algorithm for seismic traveltime inversion for 2-D velocity structures. The distance between stations and the average shot spacing were ∼7.5 km and 150 m, respectively. With several uncertainty tests he estimated an average spatial resolution of ±2.0 km for the Moho, whose position ranges from 12 to 20 km depth. Thus, the observed difference in the depth of the velocity contrast between LET and CSS techniques could lie, to some extend, in the range of uncertainties.

The distribution of the high-quality hypocentres obtained by the tomography also suggests a location of the top of the subducting plate deeper than predicted by Ye *et al.* (1996). A clear, dipping planar clustering of events between 15 and 25 km depth (Fig. 14), interpreted as interplate seismicity, corresponds to a plate interface ∼2.5 km deeper than modelled by those authors. Another factor that could explain the differences in velocity distribution between wide-angle and LET techniques is the presence of the Jacó seamount. Seamounts are highly altered and fractured oceanic crust zones, and this causes a decrease in *P*-wave velocities. This circumstance is clearly imaged in the tomograms but not in the wide-angle model (Figs 9 and 10).

Several studies using LET have been carried out in Costa Rica. Husen *et al*. (2003a) performed a country-wide LET using earthquake data from the two permanent seismological networks of Costa Rica. In the central part of the country, their model has good resolution down to 70 km depth. Their study revealed a complex lithospheric structure beneath Costa Rica, further documenting the influence of the structure and evolution of the incoming Cocos plate on the margin configuration. In general, the results presented here are in good agreement with the work of those authors. However, our model provides new insights into the first 60–70 km of this part of the subduction zone provided mainly by the offshore coverage, lacked by Husen *et al*. (2003a). In addition, observed discrepancies are attributable to the use of different reference models and model parametrizations. Absolute velocities resulting from both tomographic models are slightly different but consistent at depths greater than 10–15 km.

As imaged by Husen *et al*. (2003a), DeShon *et al*. (2006) and other previous studies in Costa Rica (e.g. Protti *et al*. 1996), the Cocos slab is a high-velocity anomaly to first order, as expected from the fact that subduction rates are more rapid than rates of thermal diffusion, yielding a slab relatively cold compared to the warm mantle. This simple image has been modified in the last years with the detection of negative anomalies along the slab in different zones of the world, such as Taiwan (Lin *et al.* 1999), Alaska (Abers, 2000; Abers *et al.* 2006) and Costa Rica (Husen *et al.* 2003a). The model of the latter authors depicts the upper part of the slab subducting beneath Central Costa Rica as a high-velocity feature with areas of low velocities appearing at different depths. In our model, on the contrary, along the Central Pacific margin we observe a continuous band of low velocities in the subducting slab starting at depths as shallow as 5–10 km at ∼5–10 km from the trench (Fig. 14), and stretching down to 60–70 km depth, were the resolution ends.

Low velocities on top of the slab have been detected by CSS methods as well. Ye *et al*. (1996) report clear near-vertical reflections from the plate interface recorded over the continental slope from their modelling of line SO81-200. They point out that their appearance requires a high-velocity contrast along the plate boundary, which they depict as a low-velocity layer slightly thicker than one km. Some 40 km further to the southeast of the area of this work, Stavenhagen *et al*. (1998) observed an upto 8-km-thick low-velocity layer overlaying the subducting slab, which possesses an increased thickness of 14 km itself. The authors attribute the thick low-velocity layer to eroded material from the margin wedge.

The appearance of low velocities inside the subducting slab can be explained by several processes taking place at different depths, in which water and the oceanic plate structure play a key role. Subduction transports large amounts of water into the Earth, including free water contained in sediments and the oceanic crust and mantle, as well as in the form of hydrous minerals. As the slab sinks, dehydration of the slab is thought to take place, releasing fluids most likely continuously, while the dehydrating lithology changes with depth from sediments, to hydrated oceanic crust, to serpentinized oceanic mantle (Ruepke *et al.* 2002). At depths greater than ∼100 km, fluids from sediments, crust and mantle are released beneath the volcanic front into the hot mantle wedge, where they may propitiate partial melting by decreasing the temperature, leading to arc volcanism. In the following, we will discuss how the different processes outlined above are expressed in our tomograms. Fig. 15 provides sketches of cross-sections 2 and 5 (Fig. 14), delineating the observed low-velocity anomalies and their interpretation.

6.1 Hydration through slab faulting

Most of the hydration of the oceanic plate seems to take place during bending near the trench, where water percolation and mineral alteration occur at extensional faulting in the crust and the upper few kilometres of the mantle (Kirby *et al.* 1996), or even deeper, 15–30 km into the mantle (Peacock 2001; Ranero *et al.* 2003, 2005). Faulting along the trench is present offshore Middle America, as imaged by high-resolution seafloor mapping, near-vertical reflection lines and outer-rise seismicity (Hinz *et al.* 1996; von Huene *et al.* 2000; Ranero *et al.* 2005; Grevemeyer *et al.* 2007). Northward from the boundary between the lithospheres formed at EPR and CNS, offshore Nicoya Peninsula, the oceanic crust is ∼5 km thick, favouring a zone of flexure and faulting wider than that to the southeast. Offshore the Central Pacific area of Costa Rica, the oceanic crust is thicker, the outer rise much smaller and the faulting in the seaward trench slope of the Cocos Plate is less developed (von Huene *et al.* 2000). Between Fisher Seamount and Quepos Plateau, the flexural stress is relieved in a narrow area by faulting along presumed zones of previous structural weakness of the plate, that is, the spreading fabric (Fig. 1). In our tomographic images, specially clear in profiles 2, 3 and 4 (Figs 14 and 15), the low-velocity layer toping the subducting slab to depths of ∼25 km appears relatively narrow, encompassing the first 5–7 km into the

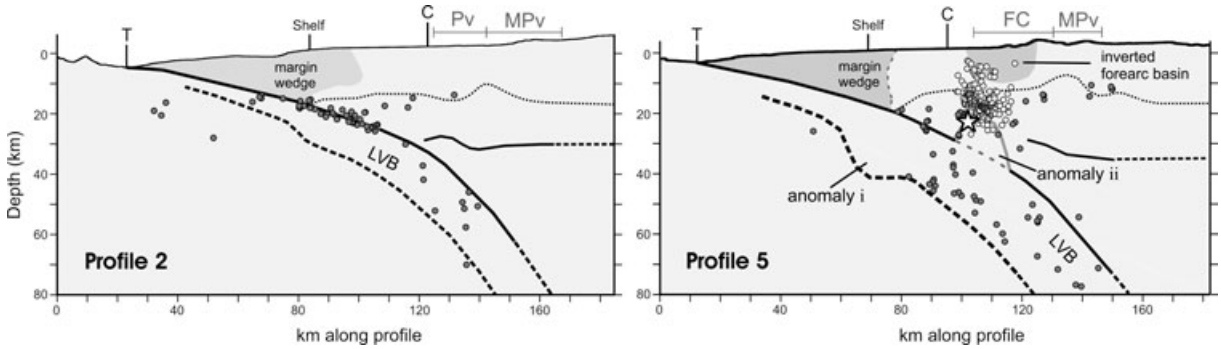

Figure 15. Schematic cross-sections through the west (profile 2) and the east (profile 5) zones of the area resolved by the Jacó array, sketching the configuration of the margin and its variation (see text for explanation). Location is given in Fig. 1. The dotted line follows the contour line of 6 km s^{-1}, which seems to represent the limit between upper and lower crust of the overlying plate. Earthquakes located within 8 km of either side are projected onto the profiles (grey circles). The topography has been slightly exaggerated, but cross-sections are at scale. The star in profile 5 represents the hypocentre of the 2004 M_w 6.4 earthquake and open circles the aftershocks (Pacheco *et al*. 2006). T and C represent the trench and coast locations, respectively. LVB: low velocity band, FC: Fila Costeña (Coastal Range), MPv: Miocene–Pliocene magmatic front and Pv: Pleistocene volcanism.

plate, in good agreement with a shallower bend-faulting. The subduction of a less deeply faulted lithosphere beneath Central Costa Rica has been invoked by Ruepke *et al*. (2002) to explain the variations in lava composition between Costa Rica, where they have been originated from a basalt-amphibolite source, and Nicaragua, where the descending lithosphere is pervasively faulted and serpentinized, favouring a deep fluid source from the slab mantle.

Another factor that could contribute to the low-velocity anomalies observed in the first kilometres of the slab is the subduction channel and the fluids stored in it. Reflection lines offshore Costa Rica (Hinz *et al.* 1996) suggest that more than 95 per cent of the sediment coverage, with a thickness of ∼0.5 km off Costa Rican Central Pacific margin, remains on the subducting plate (von Huene *et al.* 2000). The subduction erosion process adds large amounts of material removed from the upper plate to the subduction channel, introducing a layer with an estimated thickness of 400–800 m (von Huene *et al.* 2004).

6.2 Slab dehydration

At depths shallower than ∼20 km, in a low temperature environment, water is released from compaction and diagenesis of subducted sediments and the subduction channel. These fluids could migrate along the plate interface towards the trench or, most likely for erosional margins, ascend along faults formed within the upper plate by hydrofracturing on the forearc region (Ranero *et al.* 2008). High-resolution seismic records and multibeam bathymetry display pervasive normal faulting in the middle slope off Costa Rica (Ranero & von Huene 2000). The chemistry of the cold vent fluids seeping on top of the faults indicate a source at the plate interface (Hensen *et al.* 2004). The weakening of the upper-plate basement and the fluid venting, together with deformation and faulting originated by seamount subduction, justify the low velocities obtained in the margin wedge (Figs 14 and 15).

At deeper levels, from 20 to 100 km depth, progressive metamorphism releases water from sediments and oceanic crust, at pressure and temperature conditions, which are too cold to generate arc melting. The 3-D *P*-wave velocity structure and petrologic modelling from Husen *et al*. (2003a) indicate the existence of a low-velocity, hydrous oceanic crust in the subducting plate beneath Central Costa Rica. They found a good correlation between the predicted locations of hydrous minerals in the oceanic crust and the hypocentres of intermediate-depth earthquakes, supporting the hypothesis of the latter being enabled by dehydration (Kirby *et al.* 1996; Hacker *et al.* 2003; Abers *et al.* 2006). On the other hand, Ranero *et al*. (2005) present evidence from Middle America and Chile indicating that, even though dehydration embrittlement and eclogitization may contribute to stresses in the slab leading to seismogenesis, much of the intermediate-depth intraslab seismicity occurs by reactivation of old and new faults formed by plate bending near the trench. A hydrated oceanic crust explains the existence of a LVB on top of the slab down to the maximal depths resolved by this study (60–70 km) and probably beyond, at least in the west part (Fig. 14, profiles 1–2 and Fig. 15). The fact that, in this experiment, the LVB encompasses the intraslab seismicity deeper than ∼30 km (Fig. 14) agrees with slab dehydration as a seismogenic agent. Further data analysis is necessary to establish if the earthquakes are generated by dehydration embrittlement across the slab or they concentrate along pre-existent faults reactivated during subduction. For example, high-precision relative earthquake locations could eventually depict lineaments associable with faults.

As described above, the tomograms depict widening of the LVB in two senses: a vertical widening that starts at ∼25 km depth on the west portion of the margin studied here, and a general eastward widening (Figs 14 and 15). Downdip growing of the faulting downdip as the slab bends further (Mikumo *et al.* 2002; von Huene & Ranero 2003) and confronts the area, downdip of the disrupted margin wedge, where the upper plate has strengthened, may account for the vertical widening of the LVB.

6.3 Thickening of the oceanic crust

The LVB more than doubles its thickness at depths greater than ∼30 km in cross-sections 4 and 5 (Figs 14 and 15). As observed in the west zone, the intraslab seismicity distributes all over the thickened LVB (Fig. 14 profiles 4–5). Anomaly i protrudes from the bottom of the LVB, noticeable from the area crossed by profile 3 and eastward, and precedes the general downdip widening of the LVB. The shape of anomaly i resembles the structure of the seamounts imaged by this and other studies but with bigger proportions. Its appearance takes place ∼10 km closer to trench at profile 5. The onset of intraslab seismicity also draws progressively nearer to the trench, so that at profile 5 it starts ∼25 and ∼10 km seaward

from the onset at profiles 3 and 4, respectively, at least during the recording period of the Jacó network.

This eastward broadening of the LVB could be caused by the presence there of a portion of the slab displaying a more intensive, and maybe deeper, bend faulting. Nevertheless, the subduction of the Cocos Ridge and its thickened crust to the southeast suggests another origin for the widening of the LVB. Trench-parallel, wide-angle profiling ∼30 km seaward from the MAT reveals that the EPR crust offshore the Nicoya Peninsula possesses the velocity structure of normal oceanic crust (Walther & Flueh 2002). In contrast, and as expected from the presence of the Cocos Ridge, crustal thickening related to the Galapagos hotspot has been imaged all along a profile stretching from Quepos Plateau to the southeastern flank of the ridge by Walther (2003) and Sallarès *et al.* (2003). The models of those authors show a maximal crustal thickness of 19–20 km below the centre of the ridge; the thickening is almost entirely caused by a lower crust with up to three times the thickness of normal oceanic crust. Beneath the northwestern flank of the ridge, in the area of the Quepos Plateau, the CNS crust is ∼8–10 km thick (Walther 2003) or even thicker (Sallarès *et al.* 2003), the increase here being attributed to the upper crust and expressed by 3-km-thick flow basalts (Walther 2003). Velocities lower than expected for a crustal layer 2-A constituted mainly by basalts could be caused by high porosity (Walther 2003), as suggested by the slightly to highly vesicular lavas and tuffs dredged from the ridge (Werner *et al.* 1999).

Following the azimuth of the Cocos plate motion as predicted by the model Nuvel-1A (DeMets *et al*. 1994), shown in Fig. 1, a landward projection of the thickened oceanic crust existent under Quepos Plateau coincides very well with the eastward widening of the LVB (Fig. 14, profiles 4 and 5). This suggests that the widened LVB imaged by this tomography beneath the Parrita lowland and landward may be caused by the presence of subducted thickened crust with velocities in general lower than the average for normal oceanic crust. In this context, anomaly i could be interpreted as the result from hotspot activity as well, a feature similar in extension to Quepos Plateau. The velocity structure and gradient of the thickened LVB and anomaly i are very similar to those of the lower crust of Cocos Ridge as modelled by Walther (2003) and Sallarès *et al.* (2003).

Since thickened crust shows an impaired bending ability, hydration of the slab by flexural normal faulting at the trench may be decreased. Bend faulting of the Cocos Plate at the outer rise and the trench decreases southeastward and disappears against Quepos Plateau (von Huene *et al.* 2000, Fig. 1). Bathymetry highs and lithologies in the Cocos Plate, such as seamounts, the upto 900-m-thick volcaniclastic aprons extending ∼10 km on both sides of Quepos Plateau (Flores-Hernández 1996; Walther 2003), and the high-porosity flow basalts that thicken the upper crust of the plateau, may introduce some amount of water into the subduction zone, likely stored only in the first few kilometres of the slab. Yet, this and other studies (Protti *et al.* 1995a; Husen *et al.* 2003a) observe abundant intraslab seismicity in the area crossed by profiles 4 and 5 (Fig. 14) and further to the east. Even more, landward from the thicker portion of the Cocos Ridge in Southern Costa Rica, where there is no evidence of bend faulting, intraslab seismicity as deep as ∼65 km contained within a ∼20-km-thick band has been detected by a local network (Arroyo 2001). If dehydration reactions generate intraslab seismicity, alternative tectonic scenarios for hydration of the oceanic crust, such as spreading centres (Peacock 1990; Kirby *et al.* 1996) and hotspots (Seno & Yamanaka 1996), may play an important role too, at least in the case of subducted thickened crust and low-magnitude ($<M_L$ 5) seismicity.

6.4 Serpentinization of the forearc mantle wedge

The fluids released at depths from 20 to 100 km may rise buoyantly along the slab-wedge interface to hydrate the cold upper mantle wedge (Hyndman & Peacock 2003). The subduction of oceanic lithosphere reduces the temperature of the overlying forearc, providing stability conditions for hydrous serpentine minerals in the forearc mantle. Serpentinized forearc mantle may justify the aseismic nature of that portion of the subduction zone and the downdip limit of the subduction thrust earthquakes (Hyndman *et al.* 1997; Hyndman & Peacock 2003).

The model of Husen *et al*. (2003a) predicts hydrated, serpentine- and/or chlorite-bearing mantle in a narrow zone just above the subducting slab and in a larger area in the 'tip' of the mantle wedge beneath Central Costa Rica. According to empirical relationships between the degree of serpentinization and seismic *P*-wave velocities of peridotites (Carlson & Miller 2003), velocities of 7.2–7.6 km s^{-1} obtained in the narrow part of the mantle wedge resolved by this study, in the east and west zones (Fig. 14), may indicate a serpentinization of ∼5–15 per cent. This value could be slightly underestimated, given that the characteristic model test suggests an anomaly recovery of 70–80 per cent at the forearc mantle wedge. Using LET, DeShon *et al*. (2006) report a serpentinization of at least 20–25 per cent in the forearc mantle wedge beneath the Nicoya Peninsula. These results correspond well with the work of Hyndman & Peacock (2003), who examined a wide range of geophysical and geological data and concluded that serpentinization of the forearc mantle is a global expected phenomenon, commonly reaching values of 20 per cent and up to 50 per cent locally. Nevertheless, a conclusive interpretation needs the information provided by *Vp*/*Vs* modelling, which is unfortunately not available for this experiment, as mentioned before.

6.5 Subduction of ocean-bottom morphology

The configuration of the Central Costa Rican Pacific margin is modified by the subduction of seamounts, ridges and plateaus imprinted on the Cocos Plate by the Galapagos hotspot. Two subducted seamounts located upward from the seismogenic zone have been imaged by our tomographic modelling, the Jacó seamount (Figs 1, 10, 13 and 14) and ∼20 km to the southeast, at the edge of the area resolved by the LET, the Parrita seamount (Fig. 13). The latter is located ∼10 km landward from the trench axis, has a diameter of ∼18 km and is associated to the Parrita Scar (Fig. 1) on the middle margin slope. Reflection line SO81-06 previously imaged these seamounts (von Huene *et al.* 2000). Both seamounts appear as negative anomalies in the tomograms, their roots clearly signalled by a down bending of the contours of absolute velocities higher than 5 km s^{-1} in the oceanic crust and upper mantle, and an up bending of the contours of slower velocities into the margin wedge. A similar tomographic image has been obtained by Husen *et al*. (2002) for a seamount located at the entrance of the Nicoya Gulf. Discerning the summit of the seamounts in the tomogram is difficult because of the lack of velocity contrast between the top of the slab and the base of the margin wedge.

Profile 1 in Fig. 14 crosses the area where the M_w 7.0 Cóbano earthquake occurred in 1990, at the entrance of the Nicoya Gulf (Fig. 1). By analysing the source–time function of the earthquake, Protti *et al*. (1995b) suggested that it was generated by the rupture of an asperity, likely a seamount that propagated to a weaker zone. Husen *et al*. (2002) observed a tomographic low-velocity anomaly at ∼30 km depth and interpreted it as the signature of the seamount.

In our results, the absolute velocity distribution is similar to that described by those authors, but the image of the seamount is not clear. We see a slight thickening of the low velocities on top of the slab in the area, at around 20–30 km depth (Fig. 14, profile 1), but the decrease in velocity contrasts caused by the presence of the LVB and the proximity to the border of the model at this position may complicate the recognition of a seamount.

6.6 Inner forearc

Another remarkable characteristic of the portion of the margin resolved by the LET is the low-velocity anomaly ii, imaged directly over the subducting slab, from 25 to 35–40 km depth below the inner forearc, beneath Herradura and Quepos promontories (Figs 13 and 15, Fig. 14, profiles 3–5). The occurrence of this anomaly spatially coincides with the subduction of anomaly i and the thickened oceanic crust. Furthermore, the location of the anomaly closely matches the area of the subaerial forearc where differential uplift of blocks has been explained by underplating of seamounts (Fisher *et al.* 1998; Marshall *et al.* 2000; Gardner *et al.* 2001; Marshall 2007). This uplift is superimposed to the general elevation caused by the subduction of the Cocos Ridge further to the southeast, where the forearc deforms more uniformly by rapid shortening across the Fila Costeña (Kolarsky *et al.* 1995; Fisher *et al.* 2004).

Several hypothesis could explain the low velocities found underneath the inner forearc. Husen *et al*. (2003) also imaged anomaly ii in their LET and suggested that it could be a subducted seamount. Subducting seamounts offshore Central Costa Rica cause erosion and subsidence on the offshore forearc (Ranero & von Huene 2000), but several studies evidence that they travel downward unscathed (Barckhausen *et al.* 1998; von Huene *et al.* 2000; Ranero & von Huene 2000), even to depths of 20–25 km (Husen *et al.* 2002).

The concurrence of a subsiding outer forearc (Vannucchi *et al*. 2001, 2003; von Huene *et al*. 2004) and an uplifting inner forearc (Fisher *et al.* 1998; Marshall *et al.* 2000) in an erosive convergent margin could also be justified by tectonic underplating. Accretion of subducted material beneath the base of the coastal forearc since ∼2 Ma, synchronous with tectonic erosion under the trenchward part of the forearc, is described by Clift & Hartley (2007) in Peru and Northern Chile. They propose a style of non-steady state tectonic erosion in which periods of slower erosion and coastal uplift alternate with times of faster erosion and trench retreat. Such underplating has been modelled by frictional wedge analysis (Adam & Reuther 2000) and imaged as low-velocity anomaly by LET (Husen *et al*. 2000) beneath the Mejillones Peninsula in North Chile. In our case, tectonic underplating could be explained by an increase in the buoyancy of the subducting slab causing an augment in lateral stress, which propitiates an accumulation of eroded material against the base of the upper plate, at the downdip limit of the coupled interface. Velocities of 6.5–6.8 km s^{-1} modelled for anomaly ii at 25–35 km depth suggest that it may be composed of mafic igneous rocks (Christensen & Mooney 1995), probably from seamounts and the oceanic assemblages constituting the margin wedge. Removal from upper-plate material during subduction contributes enough material for underplating. Ranero & von Huene (2000) have identified two specific mechanisms of subduction erosion along the Middle America margin, namely erosion by seamount tunnelling and removal of large rock lenses of a distending upper plate. Further evidence of the undermining of the overlying plate, besides the relief disruption associated to recently subducted seamounts, is displayed by the two broad embayments affecting the upper and middle slope of the continental margin offshore the Nicoya Gulf entrance and the Parrita lowlands (Fig. 1), 45 and 70 km wide, respectively (von Huene *et al*. 2000).

Additional information for this portion of the margin is provided by the 2004 M_w 6.4 Damas earthquake (Fig. 1). According to the work of Pacheco *et al*. (2006), the main shock was located at 24 km depth, at the flank of anomaly ii as imaged by this study (Figs 13 and 15; Fig. 14, profile 5), with the aftershocks distributed between 15 and 25 km depth. The slip distribution resembles that of a simple circular rupture with a radius of 8 km, a dimension consistent with the tomographic image of anomaly ii in this area (Fig. 14, profile 5). These authors concluded that deformation takes place throughout the whole thickness of the continental crust, probably caused by seamount subduction and strong basal friction on the upper plate, caused by the subduction of the buoyant, thickened oceanic crust and underplating of large seamounts.

Nevertheless, the apparent aseismic quality of anomaly ii, inferred from Jacó records and the distribution of the 2004 earthquake aftershocks (Pacheco *et al*. 2006), may fit better on yet another scenario. The low velocities underneath the inner forearc could be explained by an accumulation of upward migrating fluids, overpressured and confined at the base of the overlying crust by the presence of the seamount or plateau and the expected increased coupling at the plate boundary. Elevated fluid pressure could increase stress on the adjacent rocks. The presence of the seamount or plateau and the thickened crust alone could justify the coastal uplift and the occurrence of the 2004 earthquake.

The hypothesis described above partially justify the coinciding observations, but if they are in effect linked, further information is needed to better constrain the interpretation. For example, *Vp*/*Vs* or *S*-wave tomography and thermal modelling could render valuable insights on the presence and distribution of fluids, improving the characterization of the different factors interacting at the margin.

7 CONCLUSIONS

We have used the *P*-wave traveltimes from 595 earthquakes recorded during 6 months by an amphibious station array, combined with information provided by controlled-source seismology profiles, to obtain a 3-D tomographic model of the shallow part of the subduction zone (<70 km) in the Central Costa Rican Pacific margin. The use of ocean-bottom stations allowed us to determine reliable hypocentres from the trench to the coast for the first time in this area.

The 3-D velocity structure of this portion of the Costa Rican margin, well resolved from the trench down to 60–70 km depth, presents a certain degree of complexity, evidenced by subducted seamounts, the transition from normal to thickened subducted oceanic crust, and possibly, tectonic underplating, taking place along a relatively short distance. This structure also reflects various processes recognized in subduction zones, invoked here to account for the observed anomalies, such as slab hydration through bend faulting, tectonic erosion and slab dehydration.

The subducting slab is resolved down to ∼70 km depth, as a high-velocity perturbation with a conspicuous band of low velocities (LVB) on top, which contains the intraslab seismicity deeper than ∼30 km. This LVB is the expression of several processes varying in depth and along the trench. From the trench down to 20–25 km depth, the low velocities encompass the first 5–7 km of the slab, originated mainly by the fault system reactivated by bending at the trench and the outer rise and by hydration (Ranero *et al.* 2005). The presence of the Jacó and Parrita seamounts locally thickens the LVB. A vertical widening of the LVB of several kilometres takes

place at around 25 km depth, roughly coinciding with the interplate seismicity above, the increase in the dipping angle, and consequently, with the augment in strength of the upper plate. Further development of the bend-faulting system under those conditions may justify the widening.

The broadening of the LVB is stronger towards the east, where it is preceded by an even sharper widening of the low velocities, interpreted as a big seamount or plateau, both with velocity structure similar to that reported for the Cocos Ridge (Walther 2003; Sallarès *et al.* 2003). The maximal thickness of the LVB concurs with the onset of the Fila Costeña (Coastal Range) onshore, considered as an inverted forearc basin (Kolarsky *et al.* 1995). We believe that this striking change represents the transition from subduction of normal oceanic crust to Galapagos-hotspot modified, thickened oceanic crust. The occurrence of intraslab seismicity distributed all over the thickened LVB suggests that slab hydration at tectonic scenarios other than the trench-outer rise may also play an important role.

The presence of the thickened crust and the accompanying big seamount or plateau shows spatial reciprocity with an aseismic low-velocity anomaly revealed beneath the inner forearc, at the base of the crust of the upper plate. This anomaly could constitute the first geophysical evidence for the tectonic underplating of seamounts and material eroded from the upper plate, previously proposed to explain the differential uplift of blocks of the inner forearc in Central Costa Rica (Fisher *et al.* 1998; Marshall *et al.* 2000). The buoyancy of the underplated material could increase crustal stress above, as indicated by the 2004 M_w 6.4 Damas earthquake (Pacheco *et al*. 2006). Alternatively, its aseismic quality suggests that the anomaly underneath the inner forearc could be caused by accumulation of upward migrating fluids, trapped at the base of the overlying crust by the presence of the seamount or plateau, which increases interplate coupling.

The margin structure presented here is the result of a relatively short recording period. The complex dynamics of subduction zones calls for longer deployment periods in order to better understand the processes and their evolution through time. Valuable information from complementing data and techniques, such as *Vp*/*Vs* modelling, attenuation, gravimetry, focal mechanism determination and geodesy, could contribute to a better characterization of the rocks physics, stress and deformation, and therefore to constrain interpretation and gain further insights into the subduction processes.

ACKNOWLEDGMENTS

We wish to thank the masters, crews and scientists of the RV Sonne and RV Meteor for their accustomed excellent performance during cruises SO163 and M54, respectively. And the GeoForschungsZentrum Potsdam for providing the equipment for the temporal land network. We thank also the superb work of personnel from ICE during installation and maintenance of the land network, as well as the people who graciously allowed us to place equipment on their properties. And T. Diehl and W. Pérez for technical support. We appreciate the suggestions and comments from two anonymous referees, the editor and L. Linkimer, which significantly improved the manuscript. Most of the figures were created with the Generic Mapping Tool (GMT) by Wessel & Smith (1998). This is contribution 155 of the SFB574 'Volatiles and Fluids in Subduction Zones' at the University of Kiel, funded by the German Research Society (DFG). I.G. Arroyo wishes to thank the German Academic Exchange Service (DAAD) for financing most of her studies in Germany, and to ETH Zurich for providing further allowance for her stay in Zurich.

REFERENCES

Abers, G.A., 2000. Hydrated subducted crust at 100–250 km depth, *Earth planet. Sci. Lett.,* **176,** 323–330.

Abers, G.A., van Keken, P.E., Kneller, E.A., Ferris, A. & Stachnik, J.C., 2006. The thermal structure of subduction zones constrained by seismic imaging: implications for slab dehydration and wedge flow, *Earth planet. Sci. Lett.,* **241,** 387–397.

Adam, J. & Reuther, C.D., 2000. Crustal dynamics and active fault mechanics during subduction erosion. Application of frictional wedge analysis on to the North Chilean Forearc, *Tectonophysics,* **321,** 297–325.

Arroyo, I.G., 2001. Sismicidad y Neotectónica en la región de influencia del Proyecto Boruca: hacia una mejor definición sismogénica del sureste de Costa Rica, *Licenciatura thesis*. Universidad de Costa Rica, Costa Rica.

Barckhausen, U., Roeser, H.A. & von Huene, R., 1998. Magnetic signature of upper plate structures and subducting seamounts at the convergent margin off Costa Rica, *J. geophys. Res.,* **103,** 7079–7094.

Barckhausen, U., Ranero, R., von Huene, R., Cande, S.C. & Roeser, H.A., 2001. Revised tectonics boundaries in the Cocos Plate off Costa Rica: implications for the segmentation of the convergent margin and for plate tectonic models, *J. geophys. Res.,* **106,** 19 207–19 220.

Baumann, M., 1994. Three-dimensional modeling of the crust-mantle boundary in the Alpine region, *PhD thesis*. ETH Zurich, Switzerland.

Bialas, J. & Flueh, E.R., 1999. A new Ocean Bottom Seismometer (with a new type of datalogger), *Sea Technol.,* **40,** 41–46.

Bilek, S.L., Schwartz, S.Y. & DeShon, H.R., 2003. Control of seafloor roughness on earthquake rupture behaviour, *Geology,* **31,** 455–458.

Carlson, R.L. & Miller, D.J., 2003. Mantle wedge water contents estimated from seismic velocities in partially serpentinized peridotites, *Geophys. Res. Lett.,* **30,** 1250, doi:10.1029/2002GL016600.

Carr, M.J. & Stoiber, R.E., 1990. Volcanism, in *The Caribbean Region, DNAG, The Geology of North America,* pp. 375–392, eds Dengo, G. & Case, J.E., GSA, Boulder, Colorado.

Christensen, N.I. & Mooney, W.D., 1995. Seismic velocity structure and composition of the continental crust: a global view, *J. geophys. Res.,* **100,** 9761–9788.

Clift, P.D. & Hartley, A.J., 2007. Slow rates of subduction erosion and coastal underplating along the Andean margin of Chile and Peru, *Geology,* **35,** 503–506, doi:10.1130/G23584A.1.

Corrigan, J., Mann, P. & Ingle, J.C., 1990. Forearc response to subduction of the Cocos Ridge, Panama-Costa Rica, *Geol. Soc. Am. Bull.,* **102,** 628–652.

DeMets C., Gordon, R., Argus, D.F. & Stein, S., 1994. Effect of recent revisions to the geomagnetic reversal timescale on estimates of current plate motions, *Geophys. Res. Lett.,* **21,** 2191–2194.

Denyer, P. & Alvarado, G.E., 2007. *Mapa Geológico de Costa Rica 2007,* scale 1:400,000, Editorial Francesa - Universidad de Costa Rica, San José, Costa Rica.

Denyer, P., Baumgartner, P.O. & Gazel, E., 2006. Characterization and tectonic implications of Mesozoic-Cenozoic oceanic assemblages of Costa Rica and Western Panama, *Geol. Acta,* **4,** 219–223.

DeShon, H.R. & Schwartz, S.Y., 2004. Evidence for serpentinization of the forearc mantle along the Nicoya Peninsula, Costa Rical, *Geophys. Res. Lett.,* **31,** L21611, doi:10.1029/2002JB002294.

DeShon, H.R. *et al*., 2006. Seismogenic zone structure beneath the Nicoya Peninsula, Costa Rica, from three-dimensional local earthquake P- and S-wave tomography, *Geophys. J. Int.,* **164,** 109–124, doi:10.1111/j.1365–246X.2005.02809.x.

Eberhart-Phillips, D., 1986. Three-dimensional velocity structure in Northern California Coast Ranges from inversion of local earthquake arrival times, *Bull. seism. Soc. Am.,* **76,** 1025–1052.

Eberhart-Phillips, D., 1990. Three-dimensional *P* and *S* velocity structure in the Coalinga region, California, *J. geophys. Res.,* **95,** 15343–15363.

Evans, J.R., Eberhart-Phillips, D. & Thurber, C.H., 1994. User's manual for SIMULPS12 for imaging *Vp* and *Vp*/*Vs*: a derivative of the Thurber tomographic inversion SIMUL3 for local earthquakes and explosions. U.S. Geol. Surv. Open-File Report, pp. 94–431, U. S. Government Printing Office.

Fisher, D.M., Gardner, T.W, Marshall, J.S., Sak, P.B. & Protti, M., 1998. Effect of subducting sea-floor roughness on fore-arc kinematics, Pacific coast, Costa Rica, *Geology,* **26,** 467–470.

Fisher, D.M., Gardner, T.W., Sak, P.B., Sanchez, J.D, Murphy, K. & Vannucchi, P., 2004. Active thrusting in the inner forearc of an erosive convergent margin, Pacific coast, Costa Rica, *Tectonics,* **23,** doi:10.1029/2002TC001464.

Flores-Hernández, A., 1996. Processing and interpretation of multichannel seismic reflection data on continental and oceanic crust of the Pacific margin of Costa Rica, *Diploma thesis*. Christian-Albrechts-Universitaet zu Kiel, Germany.

Flueh, E.R. & Bialas, J., 1996. A digital, high data capacity ocean bottom recorder for seismic investigations, *Int. Underwater Syst. Design,* **18,** 18–20.

Gardner, T.W. *et al*., 2001. Holocene fore arc block rotation in response to seamount subduction, southeastern Península de Nicoya, Costa Rica, *Geology,* **29,** 151–154.

Grevemeyer, I., Ranero, C.R., Flueh, E.R., Kläschen, D. & Bialas J., 2007. Passive and active seismological study of bending-related faulting and mantle serpentinization at the Middle America Trench, *Earth planet. Sci. Lett.,* **258,** doi:10.1016/j.epsl.2007.04.013.

Hacker, B.R., Peacock, G., Abers, A. & Holloway, S.D., 2003. Subduction factory 2. Are intermediate-depth earthquakes in subducting slabs linked to metamorphic dehydration reactions?, *J. geophys. Res.,* **108**(B1), 2030, doi:10.1029/2001JB001129.

Haslinger, F., 1998. Velocity structure, seismicity and seismotectonics of Northwestern Greece between the Gulf of Arta and Zakynthos, *PhD thesis*. ETH Zurich, Switzerland.

Haslinger, F. & Kissling, E., 2001. Investigating effects of 3-D ray tracing methods in local earthquake tomography, *Phys. Earth planet. Inter.,* **123,** 103–114.

Haslinger, F. *et al*., 1999. 3D crustal structure from local earthquake tomography around Gulf of Arta (Ionian region), NW Greece, *Tectonophysics,* **304,** 210–218.

Hauff, F., Hoernle, K., Van Den Bogaard, P., Alvarado, G. & Garbe-Schoenberg, D., 2000. Age and geochemistry of basaltic complexes in western Costa Rica: contributions to the geotectonic evolution of Central America, *Geochem. Geophys. Geosyst.,* **1,** doi:1999GC000020.

Havskov, J.L. & Ottemoeller, L., 2005. SEISAN: the Earthquake Analysis Software for Windows, Solaris and LINUX version 8.1, University of Bergen, Norway.

Hensen, C., Wallmann, K., Schmidt, M., Ranero, C.R. & Suess, E., 2004. Fluid expulsion related to mud extrusion off Costa Rica—a window to the subducting slab, *Geology,* **32,** 201–204.

Hinz, K., von Huene, R., Ranero, C.R. & the PACOMAR Working Group, 1996. Tectonic structure of the convergent margin offshore Costa Rica from multichannel seismic reflection data, *Tectonics,* **15,** 54–66.

Husen, S., Kissling, E., Flueh, E.R. & Asch, G., 1999. Accurate hypocentre determination in the seismogenic zone of the subducting Nazca Plate in Northern Chile using a combined on-/offshore network, *Geophys. J. Int.,* **138,** 687–701.

Husen, S., Kissling, E. & Flueh, E.R., 2000. Local earthquake tomography of shallow subduction in north Chile: a combined onshore and offshore study, *J. geophys. Res.,* **105,** 28 183–28 198.

Husen, S., Quintero, R. & Kissling, E., 2002. Tomographic evidence for a subducted seamount beneath the Gulf of Nicoya, Costa Rica: the cause of the 1990 Mw = 7.0 Gulf of Nicoya earthquake, *Geophys. Res. Lett.,* **29,** doi:10.1029/2001GL014045.

Husen, S., Quintero, R., Kissling, E. & Hacker, B., 2003a. Subduction-zone structure and magmatic processes beneath Costa Rica constrained by local earthquake tomography and petrological modelling, *Geophys. J. Int.,* **155,** 11–32.

Husen, S., Kissling, E., Deichmann, N., Wiemer, S., Giardini, D. & Baer, M., 2003b. Probabilistic earthquake location in complex three-dimensional velocity models: application to Switzerland, *J. geophys. Res.,* **108**(B2), 2077, doi:10.1029/2002JB001778.

Husen, S., Smith, R.B. & Waite, G.P., 2004. Evidence for gas and magmatic sources beneath the Yellowstone volcanic field from seismic tomographic imaging, *J. Volc. Geotherm. Res.,* **131,** 397–410.

Hyndman, R.D. & Peacock, S.M., 2003. Serpentinization of the forearc mantle, *Earth planet. Sci. Lett.,* **212,** 417–432.

Hyndman, R.D., Yamano M. & Oleskevich D.A., 1997. The seismogenic zone of subduction thrust faults, *Island Arc,* **6,** 244–260.

Kimura, G., Silver, E.A. & Blum, P., 1997. *Proc. of the Ocean Drilling Program Initial Reports,* **170,** pp. 458, Ocean Drill. Program, College Station, Texas.

Kirby, S.H., Engdahl, E.R. & Denlinger, R., 1996. Intermediate-depth intraslab earthquakes and arc volcanism as physical expressions of crustal and uppermost mantle metamorphism in subducting slabs, in *Subduction: Top to Bottom, Geophys. Monogr. Ser.,* pp. 195–214, eds Bebout, G.E., Scholl, D., Kirby, S. & Platt, J., AGU, Washington DC.

Kissling, E., 1988.Geotomography with local earthquake data, *Rev. Geophys.,* **26,** 659–698.

Kissling, E., Ellsworth, W.L., Eberhardt-Phillips, D. & Kradolfer, U., 1994. Initial reference models in local earthquake tomography, *J. geophys. Res.,* **99,** 19 635–19 646.

Kissling, E., Kradolfer, U. & Maurer, H., 1995. *VELEST User's Guide-short Introduction,* Institute of Geophysics and Swiss Seismological Service, ETH, Zurich.

Kissling, E., Husen, S. & Hasslinger, F., 2001. Model parameterization in seismic tomography: a choice of consequences for the solution quality, *Phys. Earth planet. Inter.,* **123,** 89–101.

Kolarsky, R.A., Mann, P. & Montero, W., 1995. Island arc response to shallow subduction of the Cocos Ridge, in *Geologic and Tectonic Development of the Caribbean Plate Boundary in Southern Central America, Special Paper 295,* pp. 235–262, ed. Mann, P., GSA, Boulder, Colorado.

Laigle, M. & Hirn, A., 1999. Explosion-seismic tomography of a magmatic body beneath Etna: volatile discharge and tectonic control of volcanism, *Geophys. Res. Lett.,* **26,** 2665–2668.

Leveque, J.-J., Rivera, L. & Wittlinger, G., 1993. On the use of the checkerboard test to asses the resolution of tomographic inversions, *Geophys. J. Int.,* **115,** 313–318.

Lienert, B.R.E. & Havskov, J., 1995. A computer program for locating earthquakes both locally and globally, *Seism. Res. Lett.,* **66,** 26–36.

Lin, C., Huang, B. & Rau, R., 1999. Seismological evidence for a low-velocity layer within the subducted slab of southern Taiwan, *Earth planet. Sci. Lett.,* **174,** 231–240.

MacMillan, I., Gans, P.B. & Alvarado, G., 2004. Middle Miocene to present plate tectonic history of the southern Central American Volcanic Arc, *Tectonophysics,* **392,** 325–348.

Marshall, J.S., 2007.Geomorphology and physiographic provinces, in *Central America—Geology, Resources, Hazards,* pp. 75–123, eds Bundschuh J. & Alvarado, G.E., Taylor & Francis/Balkema, The Netherlands.

Marshall, J.S., Fisher, D.M. & Gardner, T.W., 2000. Central Costa Rica deformed belt: kinematics of diffuse faulting across the western Panama Block, *Tectonics,* **19,** 468–492.

Marshall, J.S., Idleman, B.D., Gardner, T.W. & Fisher, D.M., 2003. Landscape evolution within a retreating volcanic arc, Costa Rica, Central America, *Geology,* **31,** 419–422.

Matumoto, T., Ohtake, M., Latham, G. & Umaña, J., 1977. Crustal structure of the Southern Central America, *Bull. seism. Soc. Am.,* **67,** 121–134.

McIntosh, K. *et al*., 2000. Large aperture seismic imaging of a convergent margin: techniques and results from the Costa Rica seismogenic zone, *Mar. geophys. Res.,* **21,** 451–474.

Mikumo, T., Yagi, Y., Singh, S.K. & Santoyo, M.A., 2002. Coseismic and postseismic stress changes in a subducting plate: Possible stress interactions between large interplate thrust and intraplate normal-faulting earthquakes, *J. geophys. Res.,* **107**(B1), 2023, doi:10.1029/2001JB00446.

Pacheco, J.F., Quintero, R., Vega, F., Segura, J., Jiménez, W. & González, V., 2006. The Mw 6.4 Damas, Costa Rica, Earthquake of 20 November 2004: aftershocks and Slip Distribution, *Bull. seism. Soc. Am.,* **96,** 1–12.

Peacock, S., 1990. Fluid processes in subduction zones, *Science,* **248,** 329–337.

Peacock, S., 2001. Are the lower planes of double seismic zones caused by serpentine dehydration in subducting oceanic mantle?, *Geology,* **29,** 299–302.

Podvin, P. & Lecomte, I., 1991. Finite difference computation of travel times in very contrasted velocity models: a massively parallel approach and its associated tools, *Geophys. J. Int.,* **105,** 271–284.

Protti, M., Güendel, F. & McNally, K., 1994. The geometry of the Wadati-Benioff zone under southern Central America and its tectonic significance: results from a high-resolution local seismographic network, *Phys. Earth planet. Inter.,* **84,** 271–287.

Protti, M., Güendel, F. & McNally, K., 1995a. Correlation between the age of the subducting Cocos plate and the geometry of the Wadati-Benioff zone under Nicaragua and Costa Rica, in *Geologic and Tectonic Development of the Caribbean Plate Boundary in Southern Central America, Special Paper 295,* pp. 309–326, ed. Mann, P., GSA, Boulder, Colorado.

Protti, M. *et al*., 1995b. The March 25, 1990 (Mw = 7.0, ML = 6.8) earthquake at the entrance of the Nicoya Gulf, Costa Rica: its prior activity, foreshocks, aftershocks, & triggered seismicity, *J. geophys. Res.,* **100,** 20 345–20 358.

Protti, M., Schwartz, S.Y. & Zandt, G, 1996. Simultaneous inversion for earthquake location and velocity structure beneath central Costa Rica, *Bull. seims. Soc. Am.,* **86,** 19–31.

Quintero, R. & Kissling, E., 2001. An improved *P-wave* velocity reference model for Costa Rica, *Geofís. Int,* **40,** 3–19.

Quintero, R. & Kulhánek, O., 1998. *Pn-wave* observations in Costa Rica, *Geofís. Int.,* **37,** 171–182.

Ranero, C.R. & von Huene, R., 2000. Subduction erosion along the Middle America convergent margin, *Nature,* **404,** 748–752.

Ranero, C.R., von Huene, R., Flueh, E.R., Duarte, M., Baca, D. & McIntosh, K., 2000. A cross section of the convergent Pacific margin of Nicaragua, *Tectonics,* **19,** 335–357.

Ranero, C.R., Phipps Morgan, J., McIntosh, K. & Reichert, C., 2003. Bending-related faulting and mantle serpentinization at the Middle America Trench, *Nature,* **425,** 367–373.

Ranero, C.R., Villaseñor, A., Morgan, J.P. & Weinrebe, W., 2005. Relationship between bend-faulting at trenches and intermediate-depth seismicity, *Geochem. Geophys. Geosyst.,* **6,** doi:10.1029/2005GC000997.

Ranero, C.R. *et al*., 2008. Hydrogeological system of erosional convergent margins and its influence on tectonics and interplate seismogenesis, *Geochem. Geophys. Geosyst.,* **9,** doi:10.1029/2007GC001679.

Reyners, M., Eberhart-Phillips, D. & Stuart, G., 1999. A three-dimensional image of shallow subduction: crustal structure of the Raukumara Peninsula, New Zealand, *Geophys. J. Int.,* **137,** 873–890.

Rivier, F., 1985. Sección geológica del Pacífico al Atlántico a través de Costa Rica, *Rev. Geol. Amér. Central,* **2,** 23–32.

Ruepke, L.H., Phipps Morgan J., Hort, M. & Connolly, J.A.D., 2002. Are the regional variations in Central American arc lavas due to differing basaltic versus peridotitic slab sources of fluids? *Geology,* **30,** 1035–1038.

Sallarès, V., Dañobeitia, J.J. & Flueh, E.R., 2001. Lithospheric structure of the Costa Rican Isthmus: effects of subduction zone magmatism on an oceanic plateau, *J. geophys. Res.,* **106,** 621–643.

Sallarès, V., Charvis, P., Flueh, E.R. & Bialas, J., 2003. Seismic structure of Cocos and Malpelo Volcanic Ridges and implications for hot spot-ridge interaction, *J. geophys. Res.,* **108**(B12), 2564, doi:10.1029/2003JB002431.

Seno, T. & Yamanaka, Y., 1996. Double seismic zones, compressional deep trench-outer rise events, and superplumes, in *Subduction: Top to Bottom, Geophys. Monogr. Ser.,* pp. 347–355, eds Bebout, G.E., Scholl, D., Kirby, S. & Platt, J., AGU, Washington DC.

Shipley, T.H., McIntosh, K.D., Silver, E.A. & Stoffa, P.L., 1992. Three-dimensional seismic imaging of the Costa Rica accretionary prism: structural diversity in a small volume of the lower slope, *J. geophys. Res.,* **97,** 4439–4459.

Stavenhagen, A.U., Flueh, E.R., Ranero, C., McIntosh, K.D., Shipley, T., Leandro, G., Schultze, A. & Dañobeitia, J.J., 1998. Seismic wide-angle investigations in Costa Rica—a crustal velocity model from the Pacific to the Caribbean, *Zbl. Geol. Palaont., Teill. 1,* **3,** 393–408.

Thurber, C.H., 1983. Earthquake locations and three-dimensional crustal structure in the Coyote Lake area, Central California, *J. geophys. Res.,* **88,** 8226–8236.

Vanucchi, P., Scholl, D.W., Meschede, M. & McDougall-Reid, K., 2001. Tectonic erosion and consequent collapse of the Pacific margin of Costa Rica: combined implications from ODP Leg 170, seismic offshore data, and regional geology of the Nicoya Peninsula, *Tectonics,* **20,** 649–668.

Vannucchi, P., Ranero, C.R., Galeotti, S.S., Straub, M., Scholl, D.W. & McDougall-Ried, K., 2003. Fast rates of subduction erosion along the Costa Rica Pacific margin: implications for nonsteady rates of crustal recycling at subduction zones, *J. geophys. Res.,* **108**(B11), 2511, doi:10.1029/2002JB002207.

Virieux, J. & Farra, V., 1991. Ray tracing in 3-D complex isotropic media: an analysis of the problem, *Geophysics,* **56,** 2057–2069.

von Huene, R. & Ranero, C.R., 2003. Subduction erosion and basal friction along the sediment-starved convergent margin off Antofagasta, Chile, *J. geophys. Res.,* **108**(B2), 2079, doi:10.1029/2001JB001569.

von Huene, R. *et al*., 1995. Morphotectonics of the Pacific convergent margin of Costa Rica, in *Geologic and Tectonic Development of the Caribbean Plate Boundary in Southern Central America, Special Paper 295,* pp. 291–307, ed. Mann, P., GSA, Boulder, Colorado.

von Huene, R., Ranero, C., Weinrebe, W. & Hinz, K., 2000. Quaternary convergent margin tectonics of Costa Rica, segmentation of the Cocos Plate, and Central American volcanism, *Tectonics,* **19,** 314–334.

von Huene, R., Ranero, C. & Vannucchi, P., 2004. A generic model of subduction erosion, *Geology,* **32,** 913–919, doi:10.1130/G20563.1.

Waldhauser, F., Kissling, E., Ansorge, J. & Mueller, S., 1998. Three-dimensional interface modelling with two-dimensional seismic data: the Alpine crust-mantle boundary, *Geophys. J. Int.,* **135,** 264–278.

Walther, C.H.E., 2003. The crustal structure of Cocos Ridge off Costa Rica, *J. geophys. Res.,* **108**(B3), 2136, doi:10.1029/2001JB000888.

Walther, C. & Flueh, E., 2002. Remnant of the ancient Farallon Plate breakup: a low-velocity body in the lower oceanic crust off Nicoya Peninsula, Costa Rica—evidence from wide-angle seismics, *Geophys. Res. Lett.,* **29,** 1939, doi:10.1029/2002GL015026.

Werner, R., Hoernle, K., van Den Bogaard, P., Ranero, C.R., von Huene, R. & Korich, D., 1999. Drowned 14 m.y. old Galapagos archipielago off the coast of Costa Rica: implications for tectonic and evolutionary models, *Geology,* **27,** 499–502.

Wessel, P. & Smith, W.H.F., 1998. New, improved version of the Generic Mapping Tools released, *EOS, Trans. Am. Geophys. Un.,* **79,** 579.

Ye, S., Bialas, J., Flueh, E.R., Stavenhagen, A., von Huene, R., Leandro, G. & Hinz, K., 1996. Crustal strucure of the Middle America Trench off Costa Rica from wide-angle seismic data, *Tectonics,* **15,** 1006–1021.

SUPPORTING INFORMATION

Additional Supporting Information may be found in the online version of this article:

We present additional information on the solution quality of the local earthquake tomography. Contains the Figs S1, S2 and S3.

Figure S1. Horizontal depth sections with solution quality assessment using synthetic checkerboard models.
Figure S2. Solution quality assessment by characteristic model test, RDE values, and resolution contours.
Figure S3. Synthetic test to examine the ability of the data to solve the observed slab structure, with a top band of low velocities of uniform thickness.

Please note: Wiley-Blackwell are not responsible for the content or functionality of any supporting materials supplied by the authors. Any queries (other than missing material) should be directed to the corresponding author for the article.